Tidal dynamics in palaeo-seas in response to changes in bathymetry, tidal forcing, and bed shear stress

Valentin Zuchuat[1*], Elisabeth Steel[2], Ryan P. Mulligan[3], Daniel S. Collins[4], J.A. Mattias Green[5]

[1]Department of Geosciences, University of Oslo, Sem Sælands Vei 1, 0371 Oslo, Norway

[2]Department of Geological Sciences and Geological Engineering, 36 Union Street, Queen's University, Kingston K7L 3N6, Ontario, Canada

[3]Department of Civil Engineering, Ellis Hall, Queen's University, Kingston K7L 3N6, Ontario, Canada

[4]International Limited, 40 Bank Street, London E14 5AB, UK

[5]School of Ocean Sciences, Bangor University, Menai Bridge, Anglesey, LL59 5AB, UK

*corresponding author: valentin.zuchuat@geo.ui.no

This paper has been submitted to Sedimentology on the 18th December 2020 for peer-review

SEDIMENTOLOGY
the journal of the International Association of Sedimentologists

Tidal dynamics in palaeo-seas in response to changes in bathymetry, tidal forcing, and bed shear stress

Journal:	*Sedimentology*
Manuscript ID	Draft
Manuscript Type:	Original Manuscript
Date Submitted by the Author:	n/a
Complete List of Authors:	Zuchuat, Valentin; University of Oslo, Department of Geosciences Steel, Elisabeth; Queen's University, Geological Sciences and Geological Engineering Mulligan, Ryan; Queen's University Department of Civil Engineering Collins, Daniel; Imperial College London, Department of Earth Science; National Institute of Advanced Industrial Science and Technology Geological Survey of Japan, Green, J.A. Mattias; Bangor University School of Ocean Sciences
Keywords:	Numerical modelling, palaeooceanography, tidal deposits, relative sea-level change, non-uniqueness, sequence stratigraphy, Upper Jurassic, Curtis Formation

Tidal dynamics in palaeo-seas in response to changes in bathymetry, tidal forcing, and bed shear stress

Valentin Zuchuat[1], Elisabeth Steel[2], Ryan P. Mulligan[3], Daniel S. Collins[4], J.A. Mattias Green[5]

[1]Department of Geosciences, University of Oslo, Sem Sælands Vei 1, 0371 Oslo, Norway

[2]Department of Geological Sciences and Geological Engineering, 36 Union Street, Queen's University, Kingston K7L 3N6, Ontario, Canada

[3]Department of Civil Engineering, Ellis Hall, Queen's University, Kingston K7L 3N6, Ontario, Canada

[4]International Limited, 40 Bank Street, London E14 5AB, UK

[5]School of Ocean Sciences, Bangor University, Menai Bridge, Anglesey, LL59 5AB, UK

Abstract

The overall goal of this study is to simulate hydrodynamic conditions in a palaeo-ocean basin in order to better understand the effects of tidal forcing on sedimentary strata and our interpretation of the rock record. The application of numerical models can help deciphering the complex temporal evolution and spatial distribution of energy in tide-dominated palaeo-ocean basins recorded within sedimentary strata. Herein, palaeotidal modelling of the epicontinental, Upper Jurassic (160 Ma, lower Oxfordian) Sundance and Curtis Seas sheds lights on the regional-scale variations in tidal dynamics as a response to possible realistic changes in ocean tidal forcing, bathymetric configuration, and bottom drag coefficient. The use of a numerical model forced with an M2 tidal constituent at the open boundary has shown that the magnitude and the location of tidal amplification, and the variability in current velocity and bed shear stress in the basin were controlled by palaeobathymetry. Second, numerical results obtained using a depth of 600 m at the ocean boundary of the system enables the prediction of a distribution of sedimentary facies similar to the one observed in the lower Curtis Formation, except in the southernmost parts of the Curtis Sea, close to the palaeoshoreline. There, the sediments could have been transported from the neighbouring arid coastal plain by aeolian processes before being reworked by tidal or alongshore currents during a subsequent transgression. In this particular scenario, the Sundance Sea and the Curtis Sea would have reached maximum depths of 240 m and 40 m respectively, which we consider to be a realistic palaeobathymetric configuration based on geological observations. In this context, the simulated 2.60 m tidal range of the Curtis Sea would classify it as a meso-tidal system. The results suggest that sedimentary successions deposited in a tide-dominated basin could be considered as non-unique since one specific succession could have been deposited under several, equally-valid relative sea-level, and/or sediment supply, and/or tidal range histories. Reciprocally, it is possible to consider sediment-supply variations and relative sea-level change (and its effects) in tide-dominated basins as non-unique, since one relative sea-level curve can lead to the deposition of different sedimentary successions in different parts of the basin. Overall,

results of our detailed numerical model indicate the need for considering the variations of tidal dynamics associated with changes in palaeobathymetric configuration when developing a geological model of a tide-dominated sedimentary basin.

Key words: Numerical modelling, palaeooceanography, tidal deposits, relative sea-level change, non-uniqueness, sequence stratigraphy, Upper Jurassic, Curtis Formation

Introduction

Tides have been observed, measured, and predicted for centuries (if not millennia) by seafarers across the world (Cartwright, 2001), despite a very limited understanding of the astronomical mechanics behind them. The first undisputable written description of tides being linked to the Moon came from Posidonius of Rhodes (Cartwright, 2001), who, during the 1st Century BCE (Before Common Era), observed the tides around today's Cadiz, in Spain. During his 30-day observation periods, he noticed two "retreats" (ebb tides) and two "invasions" (flood tides) per lunar day. He also described the correlation between the lunar cycle itself and the variations in strength of the ebb and flood tides. It is worth noting that these monthly variations in tidal strength (now known as neap-spring tides) might have been described by the Greek navigator Pytheas of Massalia three centuries earlier (Cartwright, 2001). Pytheas' book, sadly, fell into oblivion not long after publication, and the scarce evidence of his observations are only to be reported by other authors.

It is now well-understood that variations in the force of gravity caused by periodic motions of the Moon, Earth and Sun generate different components of the observed tidal water level elevations. Today, 630 tidal harmonic constituents (Simon and Page, 2017) have been identified and can be used to mathematically solve, model, and predict the propagation of modern tides, although far fewer constituents are normally used for predictions at specific locations (e.g. Fang et al., 1999; Hess, 2003; Pelling et al., 2013; Ashall et al., 2016; Kresning et al., 2019; Mulligan et al., 2019a). Of these, the semi-diurnal M2-lunar constituent is commonly the most important of them all, which, when combined with the strongest solar constituent S2, causes these neap-spring tidal cycles (Parker, 2007) that Posidonius (and Pytheas) observed centuries ago.

A plethora of evidences are preserved in the rock record testifying to the existence of ancient tides (e.g. Eriksson, 1977; Kvale & Archer, 1991; Räsänen *et al.*, 1995; Kvale, 2006; De Raaf & Boersma, 2007; James & Dalrymple, 2010; Davis & Dalrymple, 2012; Longhitano *et al.*, 2012; Gugliotta *et al.*, 2016; Rossi *et al.*, 2016; Fritzen *et al.*, 2019; Collins *et al.*, 2020; Phillips *et al.*, 2020), however some of the concepts developed from (and used in) the study of ancient tidally-influenced sedimentary strata are in contradiction with, or could be improved by, the inclusion of phenomena recognised in modern-day tidal environments (see discussion in Gugliotta & Saito, 2019; Cosma *et al.*, 2020; Finotello *et al.*, 2020). However modern tidal analogues cannot simply be directly applied to ancient systems because of changes in the Earth-Moon distance (Waltham, 2015; Meyers and Malinverno, 2018) and the distribution of continental masses on Earth, which has changed the tides and associated physical

processes through time (Green et al., 2017, 2018; Davies et al., 2020). An increased use of numerical modelling of ancient basins (e.g. Wells *et al.*, 2010; Hill *et al.*, 2011; Mitchell *et al.*, 2011; Collins *et al.*, 2018; Dean *et al.*, 2019; Green *et al.*, 2020) could help in testing hypotheses formulated from the study of the rock record, reducing discrepancies between interpreted ancient and modern tides and tidal deposits, and improving the calibration of the ancient tidal signal to adequate astronomic parameters. Complementarily, using the rock record as hard data will help constrain the model inputs and results (Ward *et al.*, 2015; Dean *et al.*, 2019; Collins *et al.*, submitted; Byrne *et al*., 2020), and exclude anomalous "numerically-viable" simulations (Ward *et al.*, 2020). In addition to these general concepts and testing static basin configurations, the combined use of field data and numerical modelling results will further help to test, quantify, and visualise the spatio-temporal changes in tidal processes resulting from changes in basin configuration (Collins *et al*., submitted). For instance, when the rock record indicates changes in relative sea level, the impact of the change in palaeobathymetric configuration (PBC) associated with these relative sea-level variations can be simulated numerically. Similarly, in depositional basins, the sedimentary record can be interpreted (Mallinson *et al*., 2018) and numerical models (Mulligan *et al*., 2020) can be used to determine confirm or enhance the knowledge of these systems. This increased knowledge of past basins will help improve understanding of how tidal processes will evolve in response to today's sea-level rise, including assisting coastal areas in their planning by demonstrating how and where the tidal regime will significantly change.

The overall aim of this paper is to better understand the environment at the time of formation and confirm geological interpretation of the rock record, by studying the impact of varying PBC, initial open-ocean tidal forcing, and bed shear stress values on the behaviour of tides across an epicontinental sea. Through a series of numerical modelling experiments, we highlight the consequences that variations in these initial conditions can have on interpreting the history and sequence stratigraphy of tidally-influenced sedimentary successions. Specific objectives are to: (i) simulate the propagation of tides in the Jurassic Sundance and Curtis seas in present day Utah, USA (Fig. 1) using a variation of potential PBC, initial open-ocean tidal forcing inputs, and bed shear stress values to assess their impact on tidal processes; (ii) carefully compare sediment distribution proxies derived from simulated flow speed and bed shear stress values (Ward *et al.*, 2015; 2020) to sedimentary data from the Upper Jurassic Curtis Formation, which corresponds to the innermost part of the Curtis Sea; and (iii) analyse the implications of these simulation results on basin history and sequence stratigraphy of similar systems.

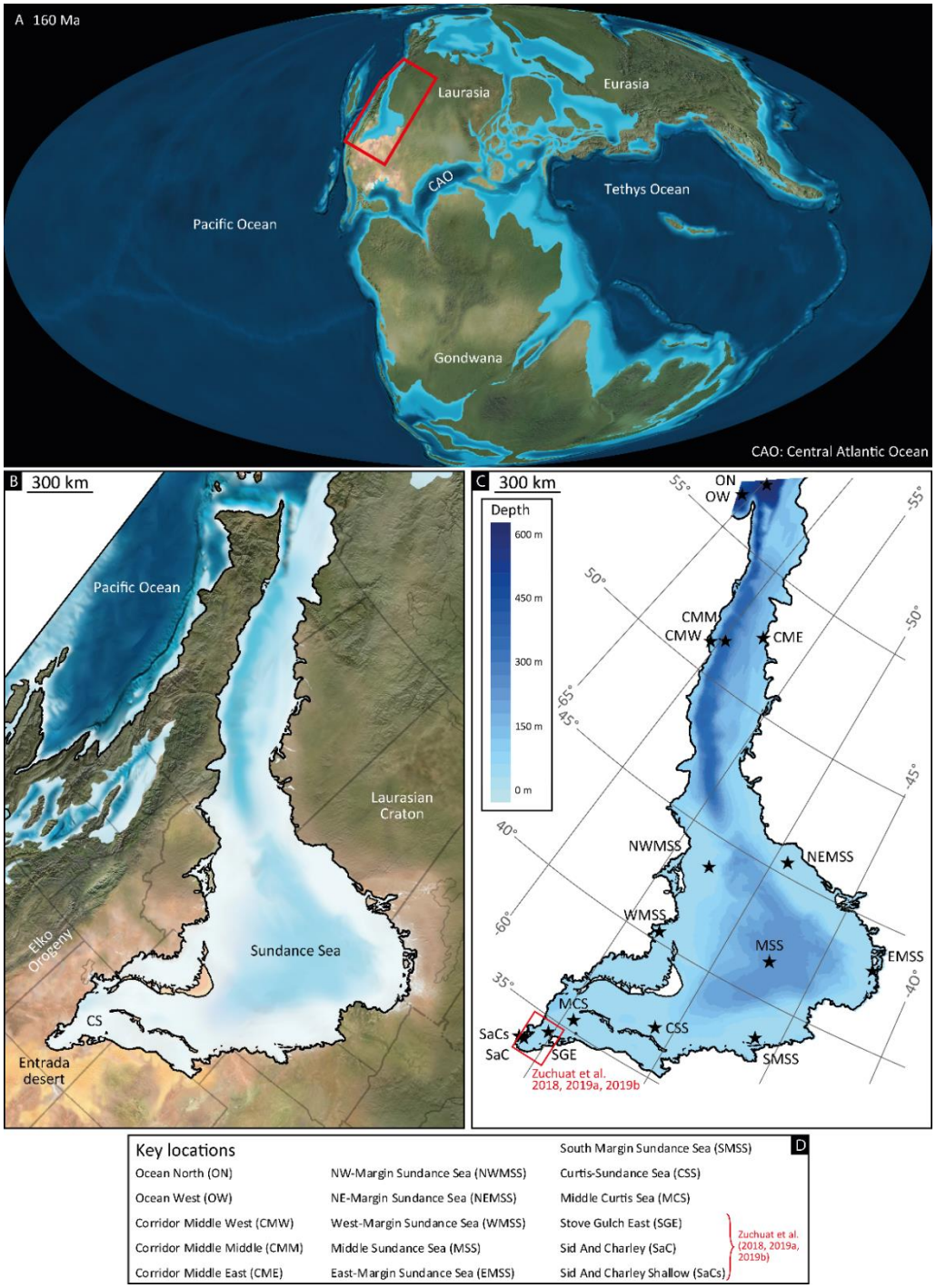

Fig. 1– A) Palaeogeographical map of the world during the Oxfordian (Lower Jurassic), 160 Ma. The red outline indicates the area of interest. B) Zoomed-in palaeogeographical map of the Sundance and Curtis Seas area. Note the presence of the Entrada Desert on the coastal plain of the Curtis Sea, potentially being the source of sediment for some of the southernmost part of the Curtis Sea. This palaeogeographical reconstruction corresponds to the time when the lower Curtis (Zuchuat et al., 2018) was being deposited (maps A and B from Blakey's Deeptime Map™, ©2016 Colorado Plateau Geosystems Inc.). C) Palaeobathymetry of the Sundance and Curtis Seas area, with a 600 m maximum depth at the mouth of the corridor, with location of the control points (D) used in this paper. The red square indicates the area surveyed by Zuchuat et al. in their 2018, 2019a, 2019b papers.

Geological context

During the Middle and Upper Jurassic, the 2500 km-long Sundance Sea (Fig. 1), also known as the proto-Western Interior Seaway (Blakey, 2014), developed in a retroarc foreland basin (Brenner & Peterson, 1994; Bjerrum & Dorsey 1995) that covered an area spanning between today's British Columbia, where it was connected to the Pacific Ocean at ~55-60°N/63-65°W, and today's Wyoming

to the SE (Imlay, 1952; Imlay, 1980; Blakey, 2014). During the Callovian and Oxfordian Stages, the Sundance Sea periodically extended an additional ~1500 km south-westward (Imlay, 1952; Pipiringos & O'Sullivan, 1978; Peterson & Pipiringos, 1979; Imlay, 1980; Kreisa & Moila, 1986; Caputo & Pryor, 1991; Anderson & Lucas, 1994; Brenner & Peterson, 1994; Peterson, 1994; Wilcox & Curie, 2008; Hintze & Kowallis, 2009; Sprinkel *et al.*, 2011; Thorman, 2011; Doelling et al., 2013; Danise & Holland, 2017, 2018; Zuchuat *et al*., 2018; 2019a; 2019b; Danise *et al*., 2020), flooding the SSW–NNE-oriented retroarc foreland basin known as the Utah–Idaho Trough (Bjerrum & Dorsey, 1995), which developed at the foot of the Elko Orogeny (Thorman, 2011; Anderson, 2015). These repeated southwestward, multi-storey incursions (Zuchuat et al., 2019a) from the Sundance Sea led to the deposition of two shallow-marine sedimentary units that crop out today in east-central Utah: The Callovian Carmel Formation and the Oxfordian Curtis Formation. The Carmel Formation (Gilluly & Reeside, 1928) primarily consists of limestone and evaporites, and was deposited as the Carmel Sea transgressed over the arid continental Temple Cap Formation (Doelling et al., 2013). The arid coastal plain deposits of the Entrada Sandstone were then deposited during subsequent regression (Crabaugh and Kocurek 1993; Peterson, 1994; CarrCrabaugh and Kocurek 1998). A second, pulsating marine transgression occurred during the Oxfordian (Wilcox & Curie, 2008; Zuchuat et al., 2019a), and led to the deposition of the siliciclastic-rich Curtis Formation (Fig. 2; Gilluly & Reeside, 1928). Recent re-examination of the J-3 Unconformity (Pipiringos & O'Sullivan, 1978) that defines the base of the Curtis Formation showed that this basal surface is instead a composite, diachronous surface sculpted by the combined efforts of aeolian deflation and tidal currents during the transgressive pulses of the Curtis Sea. The Curtis Formation is conformably overlain by arid mudflats of the Summerville Formation (Gilluly & Reeside, 1928), which developed as the Curtis Sea regressed towards the NE (Caputo & Pryor 1991; Wilcox & Curie, 2008; Zuchuat et al., 2019a).

The Carmel Formation and especially the Curtis Formation were strongly influenced by tidal currents at the time of their deposition (Fig. 3; Kreisa & Moila, 1986; Caputo & Pryor 1991; Wilcox & Curie, 2008; Doelling et al., 2013; Zuchuat et al., 2018; 2019a; 2019b). Evidence of strong tidal currents include: common heterolithic lithologies, including inclined heterolithic strata; rhythmites; tidal bundles and flaser bedding, both of which are often combined with additional indications of periodic waxing and waning of the flow; and robust sedimentary and statistical evidence of recurrent flow reversals, comprising reactivation surfaces in compound dunes (some associated with subordinate counter-current ripples at their toes), bidirectionally-accreting bar-forms, and herringbone cross-stratification.

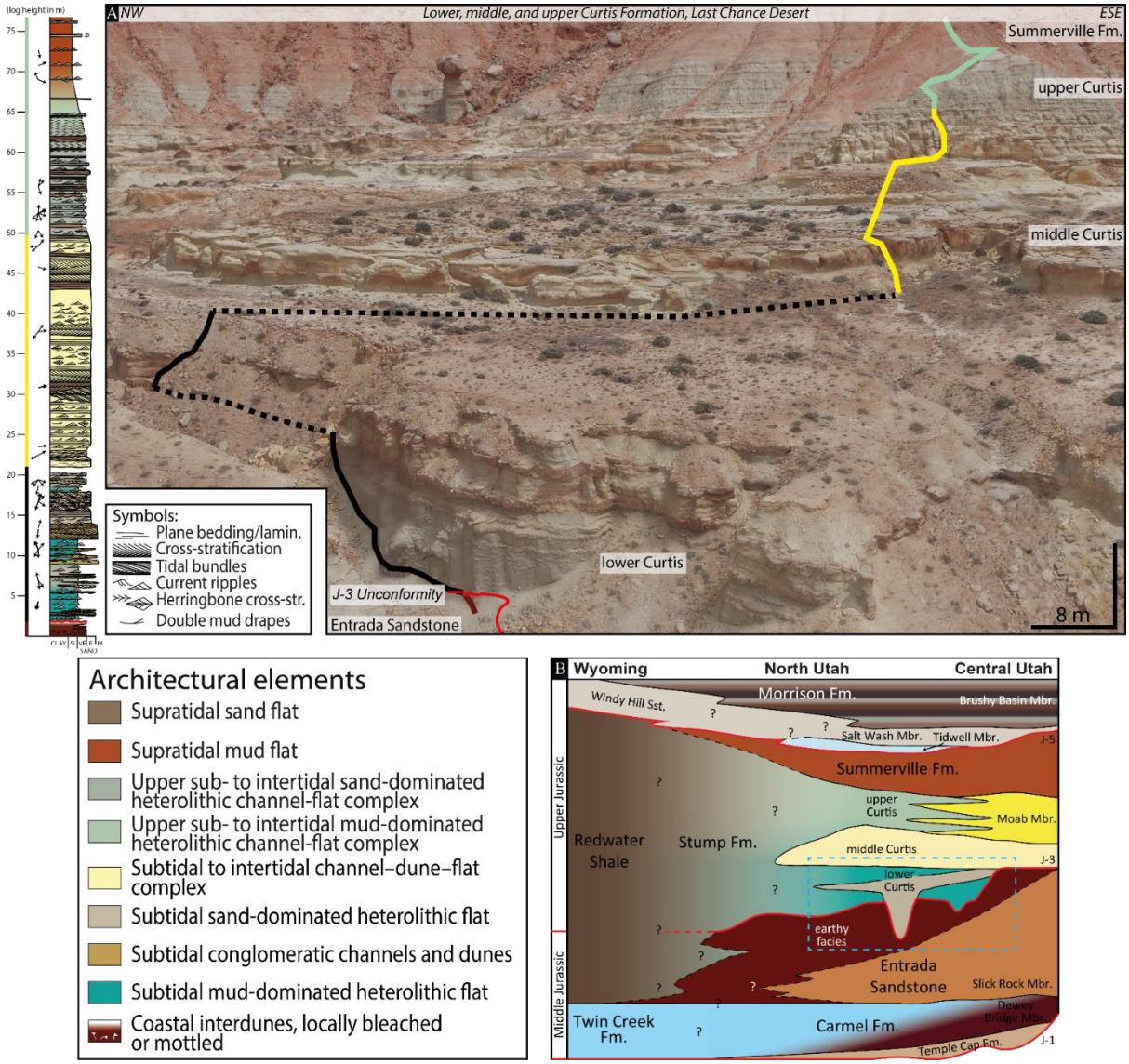

Fig. 2 – A) Photograph of the Curtis Formation accompanied by a sedimentary log detailing the stratigraphic architecture of the formation. The base of the Curtis Formation corresponds to the "J-3 Unconformity" (see Zuchuat et al., 2019a for detail discussion on the nature of this regional surface). The Curtis Formation is subdivided into three informal subunits: the thinly-bedded, heterolithic, lower Curtis (black trace), the well-sorted, cross-stratified and amalgamated, middle Curtis (yellow trace), and the fining-upward, tabular, upper Curtis (light green trace; Zuchuat et al., 2018). This paper will focus on the development of the lower Curtis only. B) Schematic panel displaying the part of the Middle and Upper Jurassic lithostratigraphy outcropping between Central Utah and Wyoming (after Doelling et al., 2013; Danise & Holland, 2017; Zuchuat et al., 2018; Danise et al., 2020). Note that the J-3 and the J-5 Unconformities are not regarded as unconformities sensu stricto anymore, but rather as a highly diachronous transgressive surface (Zuchuat et al., 2019a), and the product of a prograding braided fluvio-deltaic system unimpacted by relative sea-level fall (Danise et al., 2020), respectively.

The correlative units of the Curtis-Summerville interval towards the Sundance Sea are the Stump Formation, cropping out in the Uinta Mountains of northeastern Utah and near the Wyoming-Idaho border (Mansfield & Roundy, 1916; Pipiringos & Imlay, 1979; Imlay, 1980; Patterson-Wittstrom, 1980; Wilcox & Currie, 2008, Jensen *et al.*, 2016, Kowallis *et al.*, 2018) and the Redwater Shale Member of the Sundance Formation in Wyoming (Imlay, 1947, 1980; Patterson-Wittstrom, 1980; Uhlir *et al.*, 1988). The mudstones of the Redwater Shale Member record deposition in the deeper part of the Sundance Sea (Imlay, 1980; Danise & Holland, 2018), and thus experienced limited tidal influence. In contrast, the heterolithic Stump Formation, which mostly consists of glauconitic sandstone, muddy siltstone, and oolitic limestone (Pipiringos & Imlay, 1979; Imlay, 1980; Patterson-Wittstrom, 1980, Jensen *et al.*, 2016, Kowallis *et al.*, 2018), was influenced by tidal processes at the time of deposition

(Wilcox & Currie, 2008). The lack of high-resolution biostratigraphy and absolute dating of Curtis-Summerville interval makes precise regional correlation between units in the Curtis Sea and Sundance Sea challenging. Nevertheless, as the Oxfordian regression of the Curtis Sea persisted and the climate became more humid (Demko *et al.*, 2004; Boucot *et al.*, 2013; Danise & Holland, 2017), the shoreline developed as a tide-dominated deltaic system (Holland & Wright, 2020). These sandstone-dominated strata, which belong to the Windy Hill Member of the Morrison Formation (Pipiringos, 1968), indicate that tidal currents lingered despite a shrinking sea (Uhlir *et al.*, 1988; Danise & Holland, 2018; Holland & Wright, 2020).

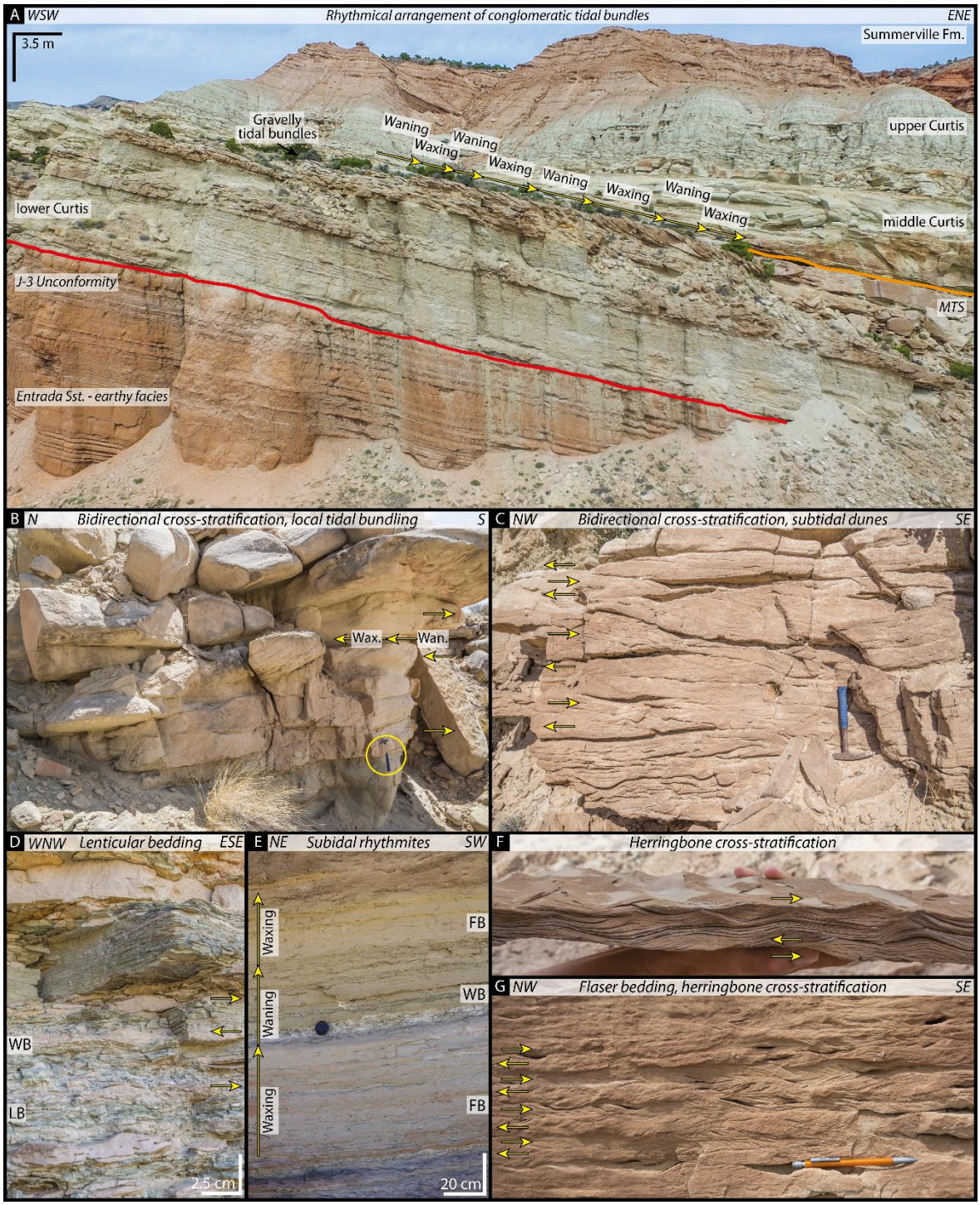

Fig. 3 – Example of sedimentary bedforms diagnostic of tidal currents (See Zuchuat et al., 2018 and 2019a for detail sedimentological description). A) Rhythmical development of conglomeratic tidal bundles following phases of waxing and waning of tidal currents. B) Bidirectional cross-stratification in stacked, three-dimensional (3D) subtidal dunes, with local

waxing-waning architecture. Hammer for scale (yellow circle, ~ 32 cm long). C) Bidirectional cross-stratification in 3D subtidal dunes. Hammer for scale. D) Heterolithic strata, deposited as lenticular (LB) and wavy bedding (WB), with bidirectional, ripple cross-stratified sandstone lenses. E) Subtidal rhythmites, testifying to phases of waxing and waning tidal currents. F) Bidirectional ripple cross-stratified sandstone bed (herringbone cross-stratification). Hand for scale. G) Flaser bedded sandstone, with bidirectional ripple cross-stratification. Pencil for scale (ca. 15 cm long).

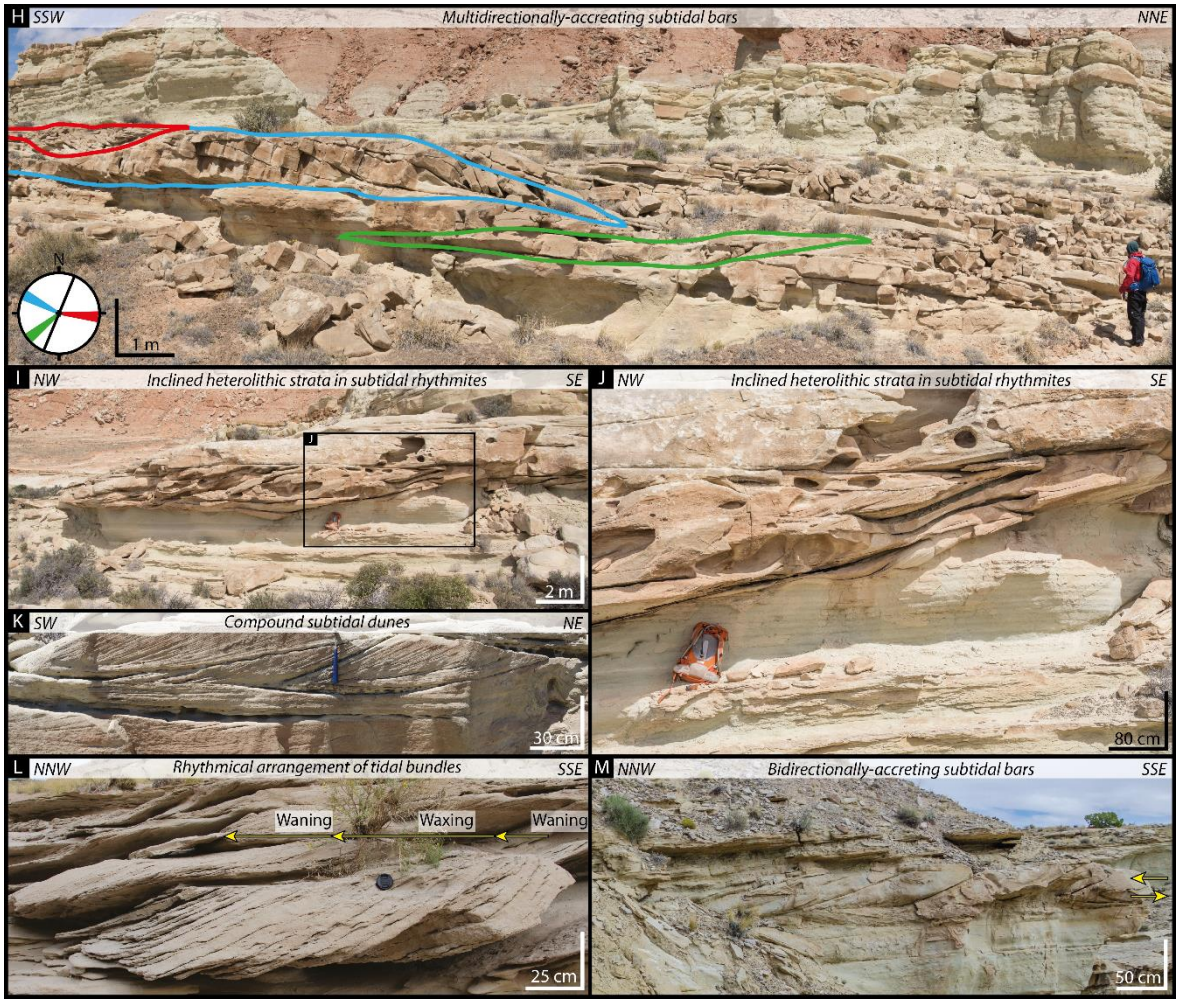

Fig. 3 (follows) – H) Colour-coded, multidirectionally-accreating subtidal bars. The black line on the rose diagram corresponds to the SSW-NNE orientation of the photograph. Geologist for scale (1.80 m). I-J) Inclined heterolithic strata, product of the lateral migration of the meander of subtidal-channel, incising into subtidal rhythmites. (Backpack for scale, height ca. 75 cm). K) Compound, 3D subtidal dune with multiple reactivation surfaces. L) Rhythmical development of sigmoidal tidal bundles following phases of waxing and waning of tidal currents. M) Bidirectional migration of subtidal bars.

Methods

Numerical Modelling

The method follows common practice for hydrodynamic modelling in present day tidal basins, however we lack observations of water levels and currents, and therefore we rely on the geological interpretations of the palaeo environmental conditions to set up the model. The modelling of tides in the Upper Jurassic Sundance and Curtis Seas used the Oxfordian palaeogeographical map from Deep Time Maps (Fig. 1), which was geo-palaeoreferenced using GPlates (Müller *et al.*, 2018). Various PBCs were then generated by converting the maps to a bathymetric raster (Python code; Appendix A) and then importing them into Deltares open-source Delft3D numerical modelling software. Delft3D is a three-dimensional (3D) hydrodynamic simulation suite, which has notably been used to model different coastal systems, including river deltas, beaches, estuaries, lagoons, and barrier islands-inlet

systems (e.g. Hu *et al.*, 2009; Elias *et al.*, 2012; Brown *et al.*, 2014; Mulligan *et al.*, 2015; Mulligan *et al.*, 2019b). Due to the unknown true water depths and the need to investigate different realistic PBC scenarios, a series of different depth grids were generated using the colour-gradient in the original paleogeographic map. The shoreline (i.e. lightest map colour) was assigned a depth of 0 m, and the mouth of the system (the darkest map colour) was assigned depths of 300 m, 460 m, 555 m, 600 m, 645 m, 860 m, 1000 m, 1200 m, and 1400 m to generate 9 different depth scenarios (note that the name of each simulation used in this manuscript refers to these maximum depth values). Each depth scenario provides a different basin slope, i.e. the shallower the depth at the mouth of the system, the shallower basin slope is, and vice-versa.

The grid used to run the simulations comprised 100'496 cells, which are approximately 3.4×3.4 km at the mouth of the system in the north, and 3.6×5.7 km in the southernmost part of the study area, which equates to cells that are 3.4-3.6 km in length, and 220 arc-seconds in width. The northern ocean boundaries were open boundaries, allowing tidal waves to enter and exit the system in a "natural fashion" and avoiding artificial reverberation. Shoreline boundaries were finite because the km-resolution of the grid would not resolve processes such the wetting and drying cycles of coastal areas.

Because it was not possible to know the exact oscillation of the water level or the specific combination of tidal constituents that affected the studied system, the idealized tides were simulated in the basin using the M2 tidal constituent with a 12.4 hr period. Therefore, even though neap-spring cycles are recognised in the Curtis Formation (Zuchuat et al., 2018, 2019a), the results of the simulations do not resolve the spring-neap oscillation. Other parameters such as the gravitational acceleration (g = 9.81 m/s^2) and fluid density (ρ = 1025 kg/m^3) were held constant.

The 9 above-mentioned depth scenarios were used to model the propagation of the M2 tides with a 1 minute time step (Fig. 4). The simulations were run for 44 days, allowing the tides to reach steady-state. Note that the simulations that used the 1430 m PBC were run for 134 days to allow the tides to reach equilibrium. It is suspected that this delay in equilibrium-reach is linked to internally generated oscillations in the basin, but this analysis extends beyond the scope of this paper. An initial tidal forcing of 0.5 m based on global simulations of the time slice (D. Hadley-Pryce, personal communication) at the mouth of the system was used to run the simulations, as well as a more extreme initial tidal forcing of 2 m, to test how the basin would respond to change in initial tidal forcing (Table 1). These 18 simulations used a "medium" drag coefficient (Cd) value of 0.002, derived from the default Chézy coefficient in Delft3D of Cz = 65 m$^{1/2}$/s (after Mulligan *et al.*, 2010) given by:

$$Cd = \frac{g}{Cz^2} \quad (1)$$

Here, g is the gravitational acceleration. Using Equation (2; Taylor, 1929), the dissipation rate D was calculated for each these 18 simulations at every step of one complete tidal cycle:

$$D = \rho\, Cd\, u^3 \quad (2)$$

Where ρ is water density, *Cd* is the drag coefficient, and *u* is the speed of the current. Subsequently, a 1-tidal-cycle-average *D*-value was calculated for each observation site in the Curtis Sea before being averaged across the Curtis Sea for each depth scenario (Table 2).

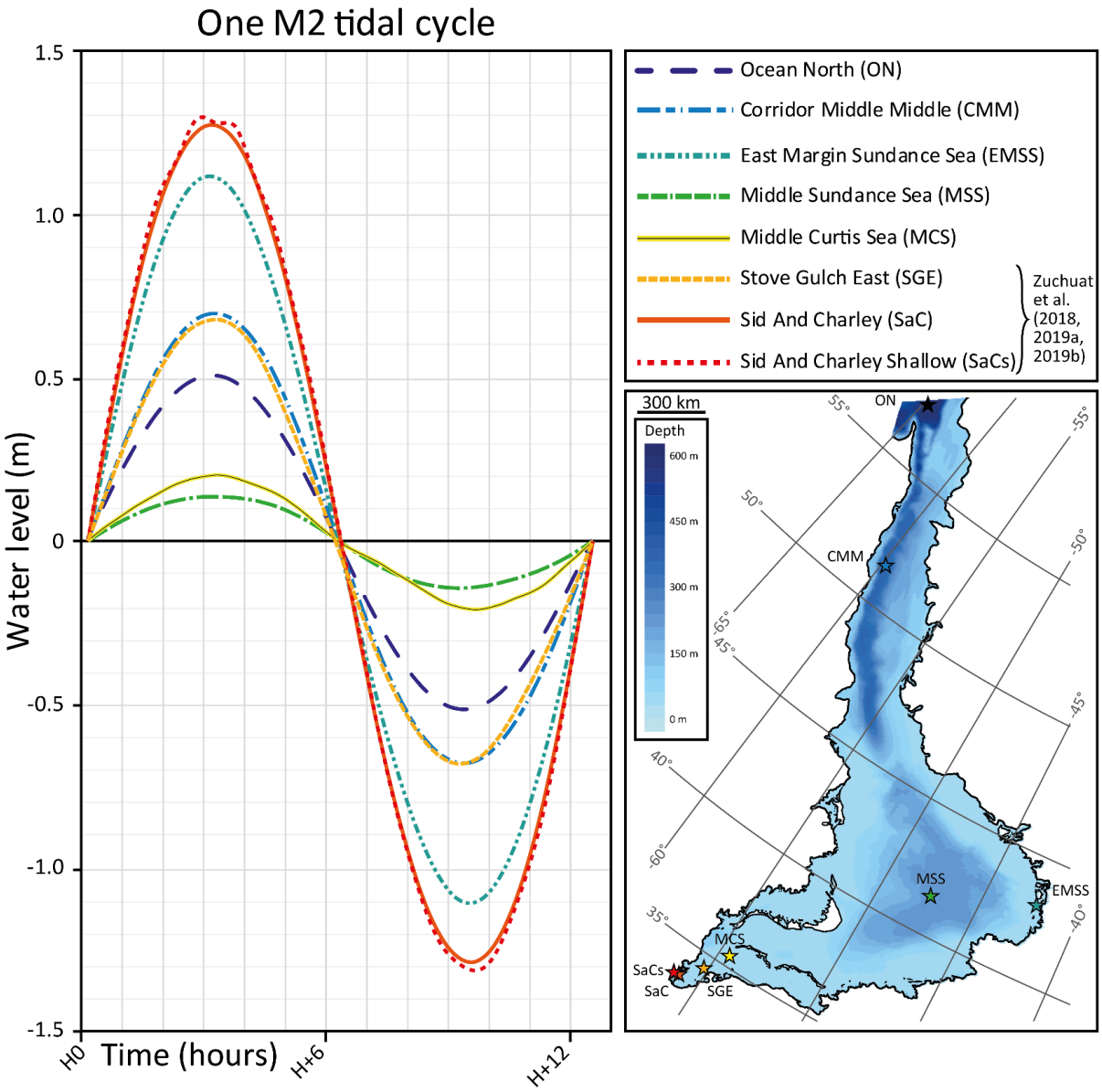

Fig. 4 – Graph showing the simulated tidal amplitude (TA) over one M2 tidal cycle at 8 key localities of the Sundance and Curtis Seas, using the 600 m PBC. With an initial open-ocean tidal forcing of 0.5 m at the mouth of the system (ON), the tides are amplified by 162% in the inner parts of the Curtis Sea, reaching 1.31 m at SaCs.

Using the 600 m depth scenario and a 0.5 m initial tidal forcing, two additional simulations were run using a high and a low *Cd*-value in order to test the sensitivity of the model to changes in the drag coefficient. The high *Cd*-value of 0.004 corresponds to $Cz = 46\ m^{1/2}/s$; and the low *Cd*-value of 0.001 equates to $Cz = 92\ m^{1/2}/s$.

Table 1 – Tidal amplitude (TA) and maximum flow speed (MFS) at SaCs and EMSS, changing as a function of varying the initial open-ocean tidal forcing.

Depth scenario	SaCs TA (m)	SaCs TA with respect to ITF (%)	Increase factor
1430 m	0.10	19.1	
1200 m	0.39	78.0	
1000 m	0.30	59.5	
820 m	0.38	76.0	
645 m	1.04	207.0	
600 m	1.31	261.0	1.45
555 m	1.11	221.9	0.87
460 m	0.57	113.0	0.76
300 m	0.30	59.0	0.68
			0.50
			0.40
			0.42
			0.56
			0.42

TA: Tidal Amplitude (m)
SaCs: Sid and Charley Shallow
ITF: Initial tidal forcing, 0.5 m = 100%

Depth scenario	SaCs TA (m)	SaCs TA with respect to ITF (%)
1430 m	0.55	27.7
1200 m	1.35	67.5
1000 m	0.90	45.2
820 m	1.04	51.8
645 m	2.06	102.8
600 m	2.10	105.0
555 m	1.87	93.5
460 m	1.27	63.5
300 m	0.50	24.8

TA: Tidal Amplitude (m)
SaCs: Sid and Charley Shallow
ITF: Initial tidal forcing, 2 m = 100%

EMSS TA (m)	EMSS TA with respect to ITF (%)	Increase factor
0.29	58.9	
0.58	115.0	
0.95	190.2	
0.45	90.0	
1.06	211.0	
1.11	221.0	0.95
0.70	139.0	0.85
0.64	127.0	0.87
0.44	87.0	1.04
		0.61
		0.51
		0.58
		0.34
		0.51

EMSS: East Margin Sundance Sea
ITF: Initial tidal forcing, 0.5 m = 100%

EMSS TA (m)	EMSS TA with respect to ITF (%)
1.12	55.8
1.97	98.3
3.31	165.4
1.87	93.3
2.57	128.5
2.25	112.5
1.61	80.5
0.87	43.5
0.89	44.5

EMSS: East Margin Sundance Sea
ITF: Initial tidal forcing, 2 m = 100%

SaCs MFS (m/s)	Increase factor
0.003	
0.01	
0.02	
0.04	
0.08	4.97
0.11	5.00
0.10	2.58
0.09	1.25
0.06	2.25
	2.09
	2.30
	2.00
	1.50

MFS: max. flow speed (m/s)

SaCs MFS (m/s)
0.015
0.050
0.047
0.050
0.180
0.230
0.230
0.180
0.090

MFS: max. flow speed (m/s)

EMSS MFS (m/s)	Increase factor
0.03	
0.07	
0.14	
0.16	
0.25	3.83
0.27	3.14
0.20	3.95
0.19	2.00
0.28	2.36
	2.15
	2.35
	1.58
	1.86

EMSS MFS (m/s)
0.107
0.220
0.534
0.320
0.590
0.580
0.470
0.300
0.520

Table 2 – Comparison between the averaged dissipation values calculated for each palaeobathymetry-scenario for a 0.5 m initial open-ocean tidal forcing and a 2.0 m open-ocean tidal forcing, showing that the dissipation rate is at least 11.5 times stronger with an initial TA four times higher. This increase factor varies significantly and non-linearly, depending on the palaeobathymetry.

Depth scenario	Basin-averaged D*, 0.5 m ITF	Basin-averaged D*, 2 m ITF	Increase factor
1430 m	0.00001	0.00076	54.56
1200 m	0.00028	0.00653	23.18
1000 m	0.00073	0.00879	12.11
820 m	0.00019	0.00701	37.51
645 m	0.00104	0.01242	11.96
600 m	0.00425	0.04915	11.55
555 m	0.00172	0.04310	25.11
460 m	0.00043	0.01057	24.44
300 m	0.00017	0.00729	43.96

* Calculated using Equations (1) and (2)
ITF: Initial, open-ocean tidal forcing

In addition to the collection of basin-wide data at every step of the simulation (Fig. 5; 6), 34 additional artificial "observation sites" were positioned across the seas to monitor and collect water level, flow speed, and bed shear stress values, of which 16 representative sites (Fig. 1) were actively used to analyse simulation results. Of these 34 observation sites, eight were employed to highlight diagnostic behaviours of the tides across the basin (Fig. 4; 7).

Simulation results

Here, we focus on the nine simulations run with an initial tidal forcing of 0.5 m (Fig. 4; 5; 6; 7). The results of the simulations run with an initial tidal forcing of 2 m are available as supplementary material (Appendix B).

Tidal characteristics, 600 m depth scenario

In the 600m scenario, the simulated tidal amplitudes (Fig 4) showed a 10-minute tidal asymmetry in most of the basin; it is only in the innermost parts of the Curtis sea that this is not the case. The asymmetry means that the ebb flow lasted 10 minutes longer than the flood flow (see figure 4).

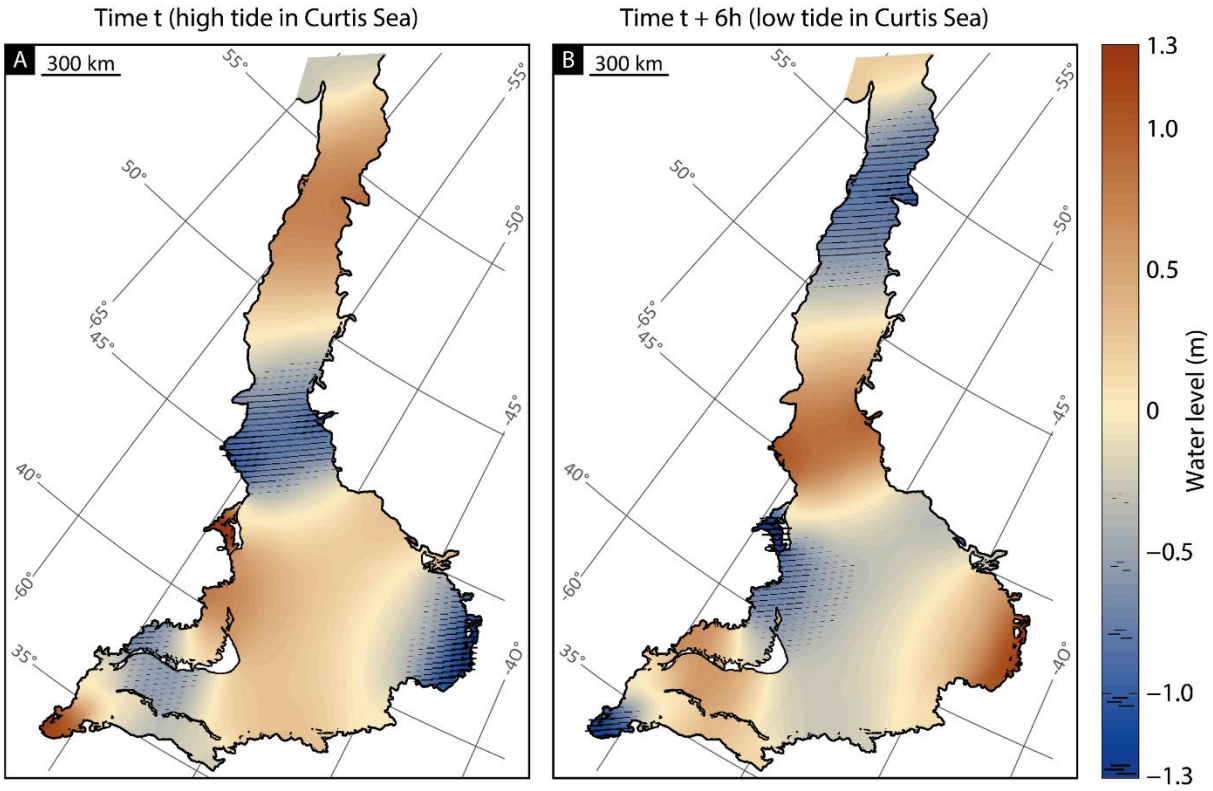

Fig. 5 – Maps showing the distribution of the water level at time t, corresponding to the high tide in the Curtis Sea, and at time t+6, corresponding to the low tide in the Curtis Sea, for the 600 m PBC, with an initial open-ocean tidal forcing of 0.5 m.

The tidal circulation in the central, southern, and eastern parts of the Sundance Sea was centred on an amphidromic point (~47°W, 43°N; Fig. 5; see also the animated abstract available with the online version of this manuscript). The area between the central part of the Sundance Sea and the Curtis Sea comprised a number of islands and inlets that separated the main water body into various sub-basins (Fig. 1). This configuration of barriers and narrow openings strongly affected the tidal propagation in this area, and hindered the development of an amphidromic circulation despite the dimensions of the basin theoretically permitting it (Fig. 5; Zuchuat et al., 2019b). The tides propagated in a rectilinear fashion along the long-axis of the Curtis Sea, which is confirmed by the sedimentary data of the Curtis Formation (Fig. 6c; 8). It is worth noting that high tide and low tide, as well as ebb tide and flood tide have a very similar magnitude with the opposite direction.

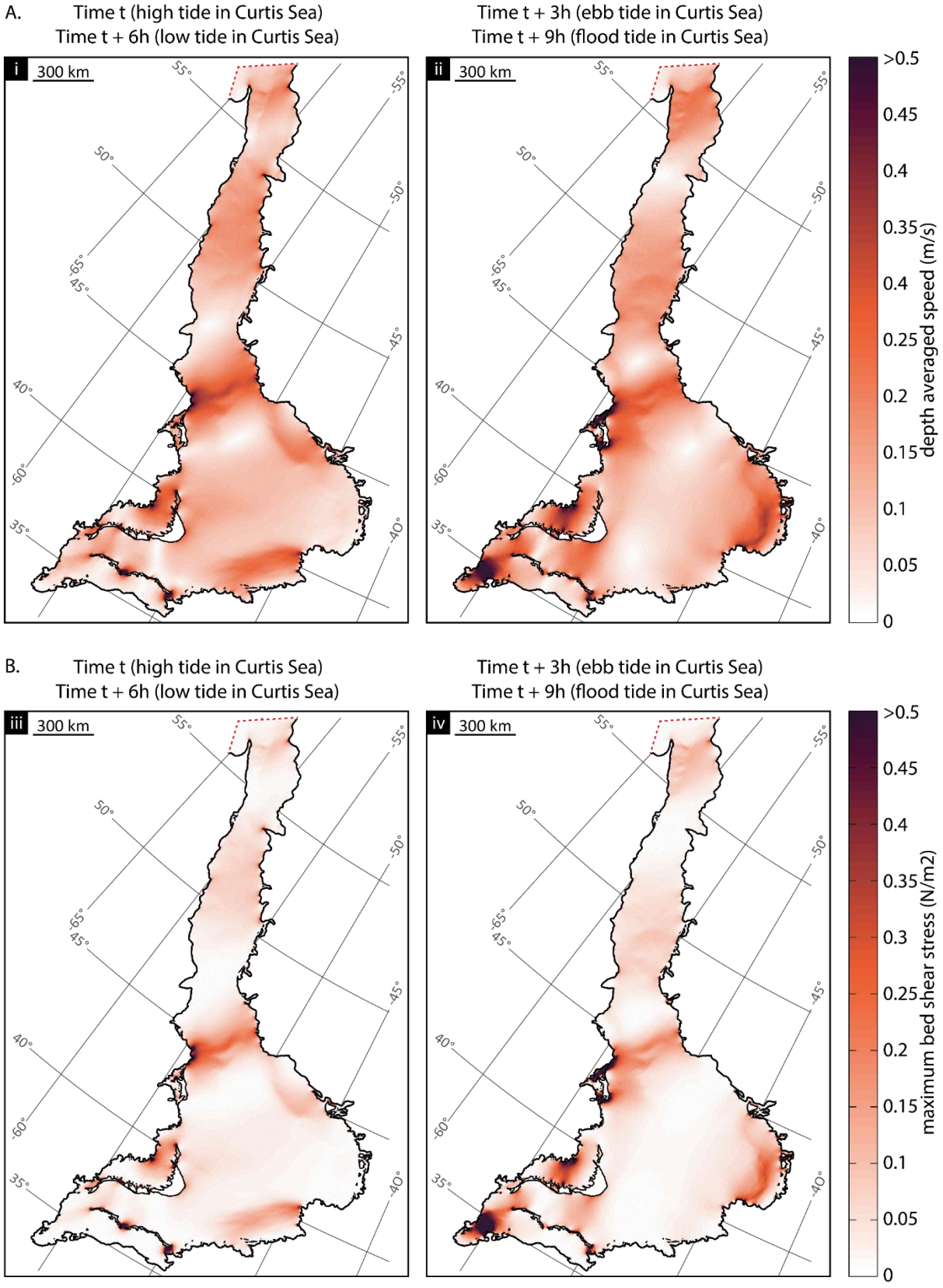
A.
Time t (high tide in Curtis Sea)
Time t + 6h (low tide in Curtis Sea)
Time t + 3h (ebb tide in Curtis Sea)
Time t + 9h (flood tide in Curtis Sea)
i
ii
300 km
depth averaged speed (m/s)
>0.5
0.45
0.4
0.35
0.4
0.25
0.2
0.15
0.1
0.05
0
B.
Time t (high tide in Curtis Sea)
Time t + 6h (low tide in Curtis Sea)
Time t + 3h (ebb tide in Curtis Sea)
Time t + 9h (flood tide in Curtis Sea)
iii
iv
300 km
maximum bed shear stress (N/m2)
>0.5
0.45
0.4
0.35
0.3
0.25
0.2
0.15
0.1
0.05
0

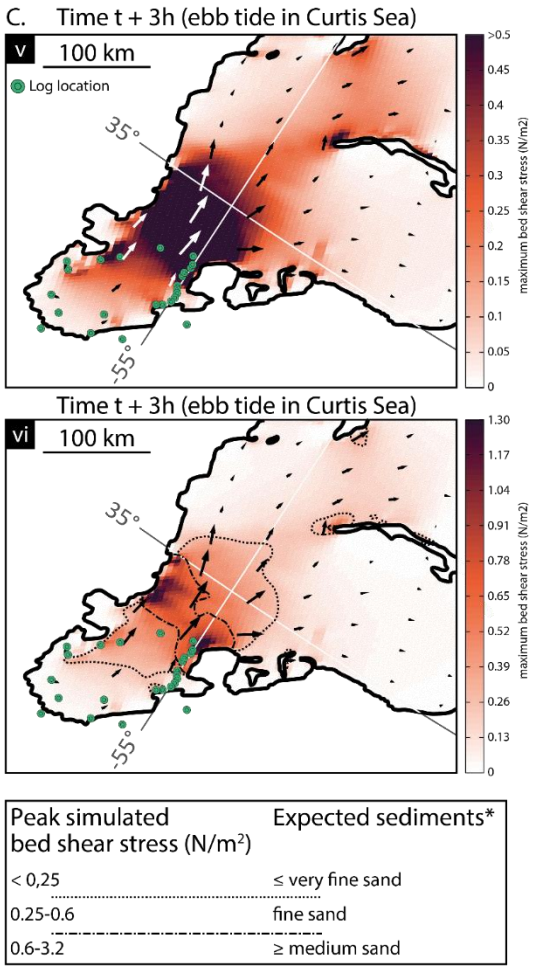

Fig. 6 – Simulation results for the 600 m PBC. A) Maps showing the distribution of the simulated depth-averaged speeds i) at time t and t+6 (high tide and low tide in the Curtis Sea, respectively), and ii) at time t+3 and t+9 (ebb tide and flood tide in the Curtis Sea, respectively). High tide and low tide were grouped together because they have a very similar magnitude with the opposite direction, and ebb tide and flood tide have been grouped together for the same reason. B) Maps showing the distribution of the simulated bed shear stress values iii) at time t and t+6 (high tide and low tide in the Curtis Sea, respectively), and iv) at time t+3 and t+9 (ebb tide and flood tide in the Curtis Sea, respectively). Cv-vi) Zoomed-in view on the Curtis Sea, showing the distribution of the simulated bed shear stress values using two different scales at time t+3 (ebb tide in the Curtis Sea) with vector arrows, as well as the locations of sedimentary logs displayed in Fig. 8. Expected sediments modified after Ward et al. (2015).

The tides at both the Curtis Sea coastline and the eastern margin of the Sundance Sea (EMSS) were characterised by an amplitude that is more than twice that of the tidal forcing at the mouth (Fig. 4), but they were out of phase: when one of the areas experienced high tides, low tides occurred in the other one (Fig. 5). Although the tidal amplitudes simulated in both areas were similar, differences occurred in maximum flow speed and basal shear stress values during their respective ebb and flow tides (Fig. 6a, 6b). Both of these values were much higher in the bottleneck of the Curtis Sea (Stove Gulch East, SGE; Fig. 6a, 6b; 7) than on the more open EMSS, indicating that the funnelling of the basin had a stronger impact on the simulated flow speed and the bed shear stress values than on the tidal amplitude. The corollary of these flow speed and bed shear stress spatial variations would be reflected in the rock record, characterised by different sediment grain sizes (Yalin & Karahan, 1979; van Rijn, 1993; Ward *et al.*, 2015; 2020) and different sedimentary architecture (Hori *et al.*, 2002; Costas *et al.*, 2011, Sleveland *et al.*, 2020) despite the similar tidal amplitudes.

Change in palaeobathymetric configuration

Changes in PBC strongly affected the resulting simulated tidal amplitude, and hence the flow speed and associated bed shear stress in the basin (Fig. 7). Certain PBCs resulted in an overall amplification of the initial tidal signal (e.g. 555 m, 600 m (strongest simulated tidal amplitude), and 645 m depth scenarios), whereas other PBCs caused these parameters to be dampened (300 m, 820 m, and 1430 m depth scenarios), or ever so slightly amplified for only a few localities (460 m, and 1200 m depth scenarios). Nevertheless, the reactivity of the system to change in PBC was not uniform across the basin. The observation sites located in the central and deeper areas of the basin (Middle Sundance Sea (MSS) and Middle Curtis Sea (MCS)) recorded a more dampened tidal amplitude with respect to the initial tidal forcing for all simulations, and their response to change in PBC was dimmer than

shallower observation sites located closer to the shoreline. For instance, at Sid and Charley (Fig. 1, SaC), tides were barely amplified with respect to the initial tidal 0.5 m forcing using the 460 m depth scenario, reaching tidal amplitude values 0.56 m (Fig. 7; see also Appendix B). Water depth at Sid and Charley increased from ~20 m to ~26 m in the 460 m and 600 m depth scenarios, respectively. This 6 m depth-increase was enough to amplify the tide to 1.28 m. Not all coastal areas responded to change in PBC in a similar manner, illustrated by the results of the 1000 m depth scenario (Fig. 7). This specific PBC led to the spatial separation of the tidal amplification in the basin: the tidal amplitude at the eastern margin of the Sundance Sea (EMSS) was nearly twice the value of the initial tidal forcing, whereas the tidal amplitude in the Curtis Sea was reduced to nearly half the value of the initial tidal forcing. Despite an increased tidal amplitude, the 1000 m depth scenario did not lead to increased flow speed and associated bed shear stress values at the EMSS. Consequently, changes in PBC controlled both the magnitude and the location of tidal amplification, as well as flow speed and bed shear stress variations in the basin. This shows the importance of bathymetry on regional tidal dynamics and further support the large-scale results in Blackledge et al (2020).

The results of these simulations suggest how the system would respond to relative sea-level variations, using the steps between each depth scenario as a proxy for relative sea-level change (Fig. 7). Starting with the shallowest basin configuration (i.e., our 300 m depth scenario), tides would first become amplified as the relative sea level increases, until the system reaches an ideal PB-configuration (the 600 m depth scenario), for which the tidal amplitudes would be at a maximum, especially in shallow areas close to the coastline. As the relative sea level keeps rising, the tidal amplitude would subsequently diminish everywhere in the basin. The deeper the basin becomes, the more heterogeneous the spatial distribution of the tidal amplitude is, resulting in different periodic resurgence of tidal amplification or dampening (Fig. 7). As a result, the stacking pattern of the various elements would strongly vary from one side of the basin to the other, despite a similar relative sea-level history.

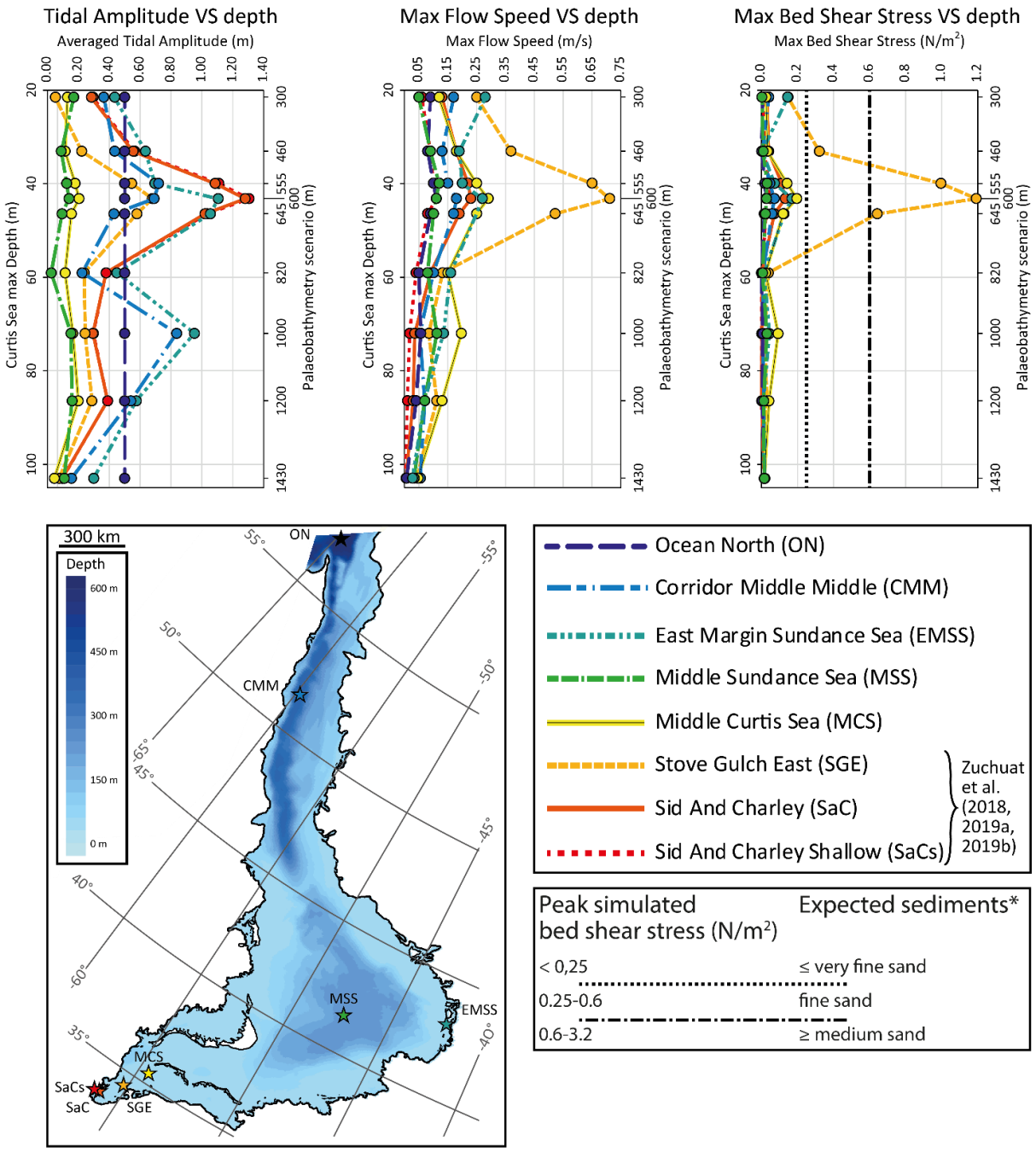

Fig. 7 – Graphs showing the simulated maximum tidal amplitudes, flow velocities, and bed shear stress at 8 key localities, for each modelled palaeobathymetry-scenario, with an initial open-ocean tidal forcing of 0.5 m at the mouth of the system (ON). Expected sediments modified after Ward et al. (2015).

Change of initial tidal forcing

Table 1 summarizes the effects of varying the tidal forcing at the open boundary from 0.5 m to 2 m, illustrated by data from SaCs and EMSS (Fig. 1; see Appendix B). The simulations were sensitive to changes in initial tidal forcing, but each location reacted differently to these variations, as illustrated by the various increase factors. Under a 555 m depth scenario, an initial tidal forcing of 0.5 m resulted in 122% amplification of the tides at SaCs, whereas initial forcing of 2 m resulted in 6.2% dampening of tides compared to the 0.5 m forcing set up (Table 1). This means that the amount of amplification at SaCs increased by a factor of 0.42 when augmenting the initial tidal forcing from 0.5 m to 2 m. Contrastingly, at EMSS, this increase factor equalled 0.58. In other words, the tidal amplitude at both

locations diminished, but it diminished differently when changing the initial tidal forcing from 0.5 m to 2 m. Furthermore, the values of these increase factors changed non-linearly when running the simulations with a different PBC, and each locality followed a different, non-linear trend (Table 1).

The evolution of the relationship between the tidal amplitude and the flow speed with respect to changes in PBC is complex (Table 1) and requires incorporating additional factors to fully decipher the true link between the tidal amplitude and the associated flow speed. At SaCs, when using an initial tidal forcing of 0.5 m, both 1000 m and 300 m depth scenarios experienced a similar tidal amplitude. However, the associated flow speed was three times higher for the 300 m depth scenario than it was for the 1000 m one. This discrepancy in flow speed was due to the different cross-sectional area of the basin between the depth scenarios: in both simulations, the same volume of water had to flow in the same amount of time. The simulated flow speed experienced using the 300 m PBC was three times higher than one experienced using the 1000 m PBC because the cross-sectional area was three times smaller.

Dissipation rate *D*

Table 2 illustrates how the dissipation rate, *D,* may likely have evolved in the Curtis Sea as a function of initial tidal forcing and PBC. Overall, an increase in initial tidal forcing always resulted in a higher rate of dissipation in the Curtis Sea, regardless of the PBC, because *D* was calculated using Equation (2). Because the use of different PBC impacted on the flow speed at each location (Appendix B), the resulting *D*-value of the Curtis Sea varied between simulations. Furthermore, since these changes in speed varied in non-linear fashion as cross-sectional dimension varies, but not the volume of water to be moved (Table 1; see also Appendix B), the changes in dissipation rate *D* evolved non-systematically as the PBC changed.

Change in drag coefficient

Changing the drag coefficient parameter, *Cd,* impacted the modelled tidal amplitude, flow speed, and bed shear stress values (Appendix C): lower *Cd* resulted in higher tidal amplitude and higher flow speeds. However, this relationship was not observed in the bed shear stress values, which followed three different trends, because of their inter dependence on *Cd* and the speed. When increasing the value of *Cd*, the bed shear stress could (i) increase, (ii) increase then decrease, or (iii) decrease. The three trends were distributed systematically across the basin: the increasing trend was recorded from the mouth of the system into the main body of the Sundance Sea, whereas the increase-decrease and the decrease trends only occurred in the Curtis Sea.

Model validation and implication for regional palaeogeography

The lowermost interval of the shallow-marine Curtis Formation (lower Curtis, sensu Zuchuat *et al.*, 2018) in east-central Utah is characterised by a specific distribution of sedimentary facies and facies associations: coarser sediments and more sand-dominated strata are concentrated in the NE and the

NW areas, whereas regions to the south generally display finer-grained, more thinly-bedded, and more heterolithic beds (Fig. 8; 9). This specific distribution of sedimentary facies and facies associations, when placed in a palaeogeographical context, shows that the coarser sediments were deposited towards the palaeo-connection between the Curtis and Sundance Seas and the NW-shoreline of the system, whereas finer sediments were deposited in the innermost parts of the Curtis Sea to the south.

As an idealized approximation, simulated bed shear-stress values can be used as a proxy to estimate the different grain sizes of the sediments being deposited by tidal processes (Ward *et al.*, 2015; Ward *et al.*, 2020): the higher the bed shear stress, the coarser the sediments (Fig. 8). The distribution of the bed shear-stress values in the Curtis Sea for the 600 m PBC (Fig. 6c) showed a very similar trend in comparison to the observed sediment grain-size distribution, especially during ebb and flood tides: the highest values were concentrated towards the palaeo-connection between the Curtis and Sundance Seas to the NE, as well as along the NW-shoreline of the system. The innermost parts of the Curtis Sea to the south were characterised by lower bed shear-stress values, implying that finer-grained sediments would be deposited there, which correspond to the field observations (Fig. 8; 9).

Nevertheless, the model did not match all outcrop localities. Though the model could explain the sedimentary architecture of the lower Curtis in the northern and western parts of the study area, it failed, on the other hand, to explain the southward-coarsening trend observed in the geology towards the innermost parts of the Curtis Sea (Fig. 8; 9). The model predicted that the sediments in these southern areas could not be coarser than very fine sand (Fig. 6c, 8, 9), but the lower Curtis in these southern areas consists mostly thinly-bedded strata made of fine-grained sand (Fig. 8; 9), and display diagnostic tidal signatures (Kreisa & Moila, 1986; Caputo & Pryor 1991; Wilcox & Curie, 2008; Zuchuat *et al.*, 2018). Such discrepancies between the simulated sediment distribution and the geological record in the southern areas of the Curtis Sea could be an artefact of the model's simplicity, which only integrated the M2 tidal constituent, as well as grid-resolution too big to render the effect of local features developing in these areas (including bedforms, channels, relief, etc.).

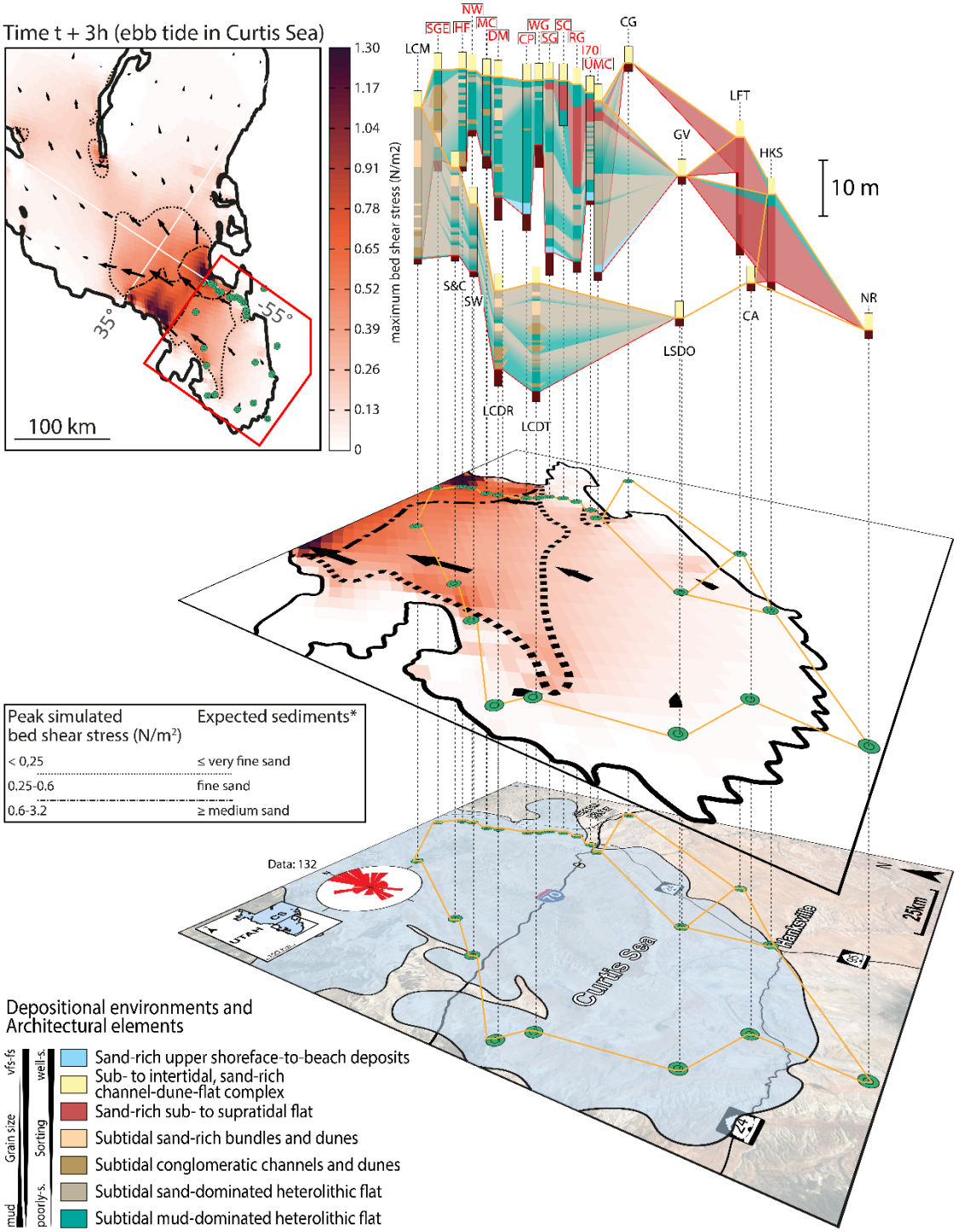

Fig. 8 – Fence diagram showing the distribution of the different facies associations and prominent architectural elements in the lower Curtis, draped onto the maximum-bed-shear-stress map at time t+3 (ebb tide in the Curtis Sea), and simplified palaeogeographical map of the Curtis Sea. The rose diagram indicates measured palaeocurrent direction in the lower Curtis. Location abbreviations, from the N, clockwise: SGE: Stove Gulch East; HF: Humbug Flats East; NW: Neversweat Wash; MC: Middle Canyon; DM: Dry Mesa; CP: Curtis Point; WG: Wet Gulch; SG: Sven's Gulch; SC: Smith's Cabin; RG: Rabbit Gulch; I70: Interstate 70; UMC: Uneva Mine Canyon; CG,: Crystal Geyser; GV: Goblin Valley; LFT: Little Flat Top; HKS: Hanksville; NR: Nottom Ranch; CA: Caineville Airstrip; LSDO: Lower South Desert Overlook; LSDT: Last Chance Desert Tower; LSDR: Last Chance Desert Road cut; SW: Saltwash View Area; SaC: Sid and Charley; LCM: Lower Cedar Mountain. Locations in red are displayed in a more detailed correlation panel in Fig. 9. Expected sediments after Ward et al. (2015).

These differences between the geology and the model could also suggest that sediment in the innermost parts of the Curtis Sea was transported and deposited by other processes (e.g. wind, or flash floods; Anthony *et al.*, 2010; Blanchard *et al.*, 2016; Rivers *et al.*, 2020), but whose signature(s) were not necessarily preserved in the rock record because tidal currents could have overprinted the original sedimentary structures. Indeed, small relative sea-level changes in low-gradient basins lead

to the migration of facies belts over large horizontal distances (Midtkandal & Nystuen, 2009; van Yperen *et al.*, 2019). The effects associated with the migration of the facies belt can be further amplified in arid, paralic environments, when these relative sea-level variations are associated with arid-humid climatic oscillations (Mountney, 2006; Anthony *et al.*, 2010; Jordan & Mountney, 2010, 2012; Blanchard *et al.*, 2016; Vieira *et al.*, 2017). Increased periods of aridity facilitate the deposition and progradation of sand flats and aeolian dunes, which can subsequently be reworked by tidal currents as the sea transgresses the previously-exposed coastal areas (Anthony & Dobroniak, 2000; Anthony *et al.*, 2010).

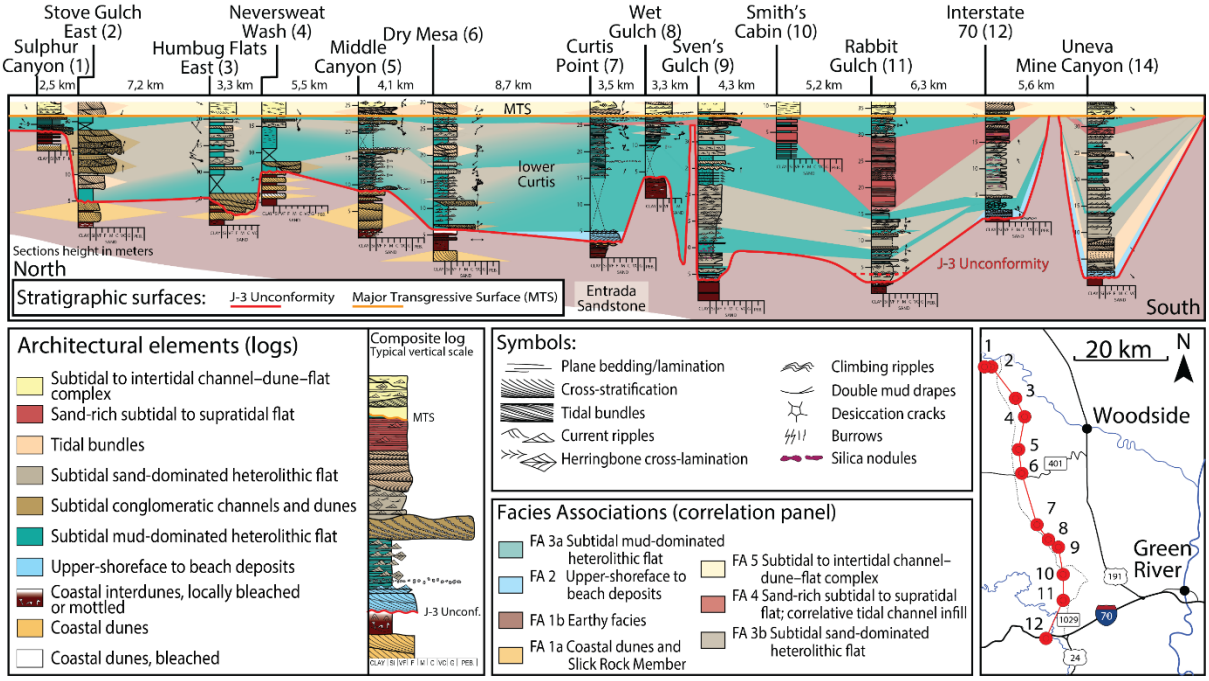

Fig. 9 – Correlation panel of the lower Curtis across the NE margin of the San Rafael Swell, showing the distribution of the different facies association (see Zuchuat et al., 2018 for detailed sedimentological descriptions).

As absolute water-depth information is lacking for the Sundance and Curtis Seas, we propose that the 600 m PBC could be considered a realistic depiction of the basin configuration during the earliest Oxfordian when the lower Curtis was being deposited (*sensu* Zuchuat et al., 2018), based on the simulation results and the similarities between the modelled sedimentary proxies and the the outcropping geology. The Sundance Sea would have therefore reached a maximum depth of ~240 m, and the seafloor of the Curtis Sea would have laid 40-45 m below the surface. In this context, the 2.60 m tidal range of the Curtis Sea would classify it as a meso-tidal system.

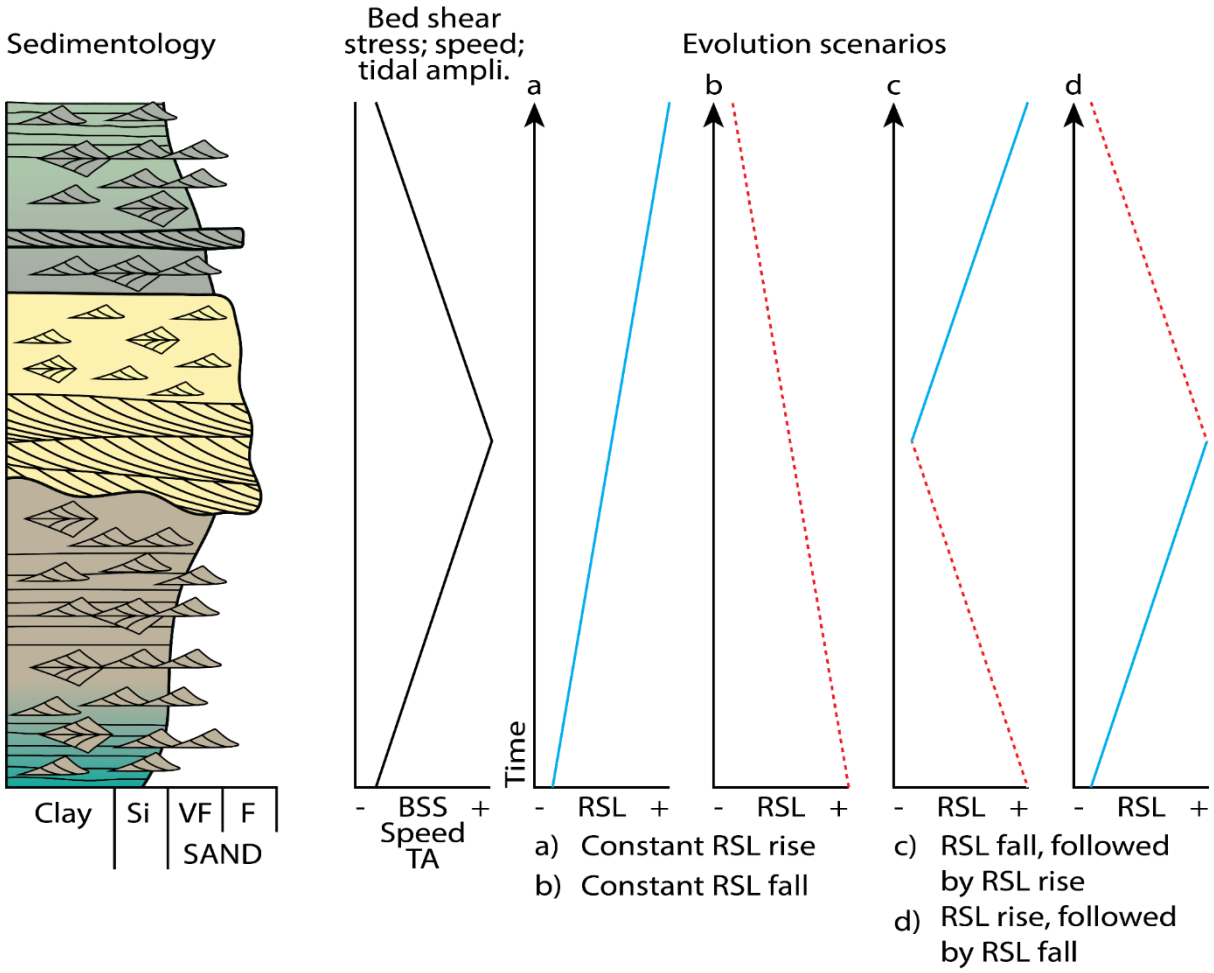

Fig. 10 – Schematic log of a hypothetical tide-dominated sedimentary column from SaCs, showing a coarsening-upward trend, followed by a fining-upward trend. According to the simulation results, the sedimentology alone, in a tide dominated environment, does not reflect a specific relative sea-level (RSL) history, as four different RSL scenarios can lead to the exact same sedimentological column. BSS: bed shear stress; TA: tidal amplitude.

Discussion

Impact on sequence stratigraphy of tide-dominated basins

The spatial distribution of sedimentary facies in tide-dominated environments is usually characterised by finer-grained sediments deposited along the coastline, in shallow water, whereas coarser sediments are deposited at greater water depth (Dalrymple *et al.*, 2012; Fan, 2012). This implies that, when the coastline progrades and the water depth diminishes, the resulting vertical sedimentary succession displays a fining-upward trend. However, this infers that the tidal dynamics in the system remains constant, despite obvious changes in the physiography of basin.

Figure 10 displays a schematic sedimentary log with a lower coarsening-upward interval overlain by a fining-upward succession (referred to as one CU2FU package). This hypothetical-sedimentological succession was deposited at SaCs in the Curtis Sea. The lower CU-interval was deposited during a period of waxing energy, with increasing tidal amplitude, flow speed, and bed shear stress values, while the upper FU interval testifies of a subsequent period of constant waning energy. Following the "classic" tidal facies model (Dalrymple *et al.*, 2012; Fan, 2012), such an energy evolution trend (and the resulting sedimentary succession) would have been deposited under a first period of relative sea-

level rise, followed by a period of relative sea level fall (or a relative sea-level standstill associated with coastal progradation). This schematic sedimentary succession (Fig. 10) could also have been deposited under a constant rate of relative sea-level rise, but with a varying rate of sediment supply. Using the "classic" tidal facies model (i.e. coarsening up = deepening up, and fining up = shallowing up; Dalrymple *et al.*, 2012; Fan, 2012), the lower, coarsening-upward part of Figure 10's section, which reflects a deepening of the basin, would have been deposited as the rate of relative sea-level rise would have outpaced the rate of sediment supply, associated with a landward migration of the shoreline (Helland-Hansen & Martinsen, 1996; Helland-Hansen & Hampson, 2009). Contrastingly, the upper, fining-upward part of the section, which reflects a shallowing of the basin, would have been deposited as a rate of sediment supply that would have outpaced the rate of relative sea-level rise, leading to the progradation of the coastline. Focusing solely on relative sea-level variations for the sake of the argument's simplicity (but acknowledging that variations in sediment supply would add an extra dimension to the complexity of the problem), the results of the simulations presented in this study (Fig. 7) indicate that this schematic sedimentary succession could reflect four, completely different, relative sea-level histories. This particular sedimentary succession could be the product of (i) a relative sea-level rise-then-fall cycle (Fig. 10c; or a relative sea-level rise followed by a period of relative sea-level standstill associated with coastal progradation); (ii) a relative sea-level fall-then-rise cycle (Fig. 10d); (iii) a constant relative sea-level rise (Fig. 10a); (iv) or a constant relative sea-level fall (Fig. 10b). In these two latter cases, the coarsest sediments would have been deposited when the physiography of the basin reached an optimal configuration that allowed tidal energy to be the most amplified, and potentially even reflecting the development of a resonant stage. Consequently, it is possible to consider such a sedimentary succession as non-unique (*sensu* Burgess & Prince, 2015), as one specific succession could have been deposited under several, equally valid relative sea-level histories. Future work will help improve the understanding of the transition from a non-resonant to a resonant stage in ancient, tide-dominated systems such as the Curtis Sea.

Greenberg *et al.* (2012) and Arns *et al.* (2015) showed that even a minor increase in relative sea level leads to a non-linear increase in tidal amplitude combined with a lower tidal energy dissipation, especially in coastal areas close to tidal resonance. But these changes are expressed differently depending on how the local physiography, the associated dissipation of tidal energy, and resonance properties of the basin evolve with respect to relative-sea level fluctuations (e.g. Ward *et al.*, 2012; Pelling *et al.*, 2013; Carless *et al.*, 2016; Idier *et al.*, 2017). The results of the simulations presented in this article confirm that the Sundance and the Curtis Seas would have experienced the same spatial-dependence of tidal processes variations with respect to relative sea-level change (Fig. 7).

Considering the CU2FU trend of the schematic sedimentary section in Figure 10, and assuming that this succession was deposited under constant relative sea-level rise, this same constant relative sea-level rise would have resulted, on the EMSS at a similar depth (Fig. 1), in the deposition of two CU2FU packages overlying each other, as the physiography of that part of the basin would have reached a

resonance-prone configuration twice (Fig. 7). Note that such a hypothetical section from the EMSS could reflect up to 16 different relative sea-level histories. This exercise is non-trivial, because it illustrates the fact that in a basin in which tides are one of the major transport and depositional processes, one particular relative sea-level history will result in the deposition of different sedimentary successions in different parts of the basin despite similar water depth, as they will reach a resonant-prone configuration at different moments in the basin's history. Consequently, in a tide-dominated basin, it is possible to consider relative sea-level change and its effect(s) as non-unique (*sensu* Burgess & Prince, 2015).

Conclusions

Evidence of tidal processes can commonly be observed in the rock record. Some recent research on modern tidal environments has highlighted the complexity of these systems (Gugluitta *et al.*, 2017; Cosma *et al.*, 2020; Finotello *et al.*, 2020). This increased understanding of modern systems is one way to improve the recognition and the interpretation of ancient tides (see discussion in Gugliotta and Saito, 2019). In addition to including insight from modern environments, the use of numerical modelling (e.g. Collins *et al.*, 2018) can help confirm (or disprove) certain hypotheses formulated from the study of the rock record. It can also help in tuning ancient tidal signals to adequate astronomic parameters, which have changed through time (Green et al., 2017, 2018; Davies et al., 2020).

The use of numerical modelling of the Upper Jurassic Sundance and Curtis Seas allowed us to quantify and constrain some of the tidal characteristics observed in the Upper Jurassic Curtis Formation (e.g. Kreisa & Moila, 1986; Caputo & Pryor 1991; Wilcox & Curie, 2008; Doelling et al., 2013; Zuchuat et al., 2018; 2019a; 2019b), and to document the influence of varying PBC, initial tidal forcing, and bed shear stress values on the behaviour of tides across epicontinental seas.

In the present study, the results of the simulations of M2 tides in the Sundance and Curtis Seas showed that:

- Changes in PBC controlled both the magnitude and the location of tidal amplification, as well as flow speed and bed shear stress variations in the basin. The magnitude and the location of tidal amplification, as well as flow speed and bed shear stress variations in the basin were also impacted by changes in initial tidal forcing and bottom drag coefficient. Changes in initial tidal forcing and bottom drag coefficient had a lesser impact on the tidal dynamics of the system in comparison to the impact of change in PBC.
- Simulation results obtained using the 600 m depth scenario predicted a distribution of sedimentary facies similar to the one observed in the lower Curtis Formation, except in the southernmost parts of the Curtis Sea, close to the palaeoshoreline, where sediments might have been transported from the neighbouring arid coastal plain by aeolian processes, before being reworked by tidal currents during a subsequent transgression.

- The 600 m depth scenario can be considered a realistic PBC for the Sundance and Curtis Seas. The Sundance Sea would have therefore reached a maximum depth of ~240 m, and the seafloor of the Curtis Sea would have reached maximum depth of 40-45 m. In this context, the simulated 2.60 m tidal range of the Curtis Sea would classify it as a meso-tidal system (2x 1.30 m tidal amplitude).
- Sedimentary successions deposited in a tide-dominated basin could be considered as non-unique (*sensu* Burgess & Prince, 2015), as one specific succession could have been deposited under several, equally-valid relative sea-level histories. Reciprocally, it is possible to consider relative sea-level change and its effect(s) as non-unique as well, since one relative sea-level curve led to the deposition of different sedimentary successions in different areas of the basins but in similar context.

Sedimentary successions deposited in tide-dominated basins reflect the energy level and the degree of tidal amplification (or dampening) that prevailed at the time of deposition. Studying these successions can help in recognising how and when certain basins reached optimal physiographic configurations for tides to be amplified. Comparing different successions can help to decipher the spatiotemporal evolution of the energy level of a basin. These changes in energy level can be related to relative sea-level variations (m to decametre scale) or change in sediment supply, but additional proxies should be considered to robustly interpret the true relative sea-level variations recorded by tide-dominated basins. Consequently, caution is required, and several possible interpretations should be considered when developing a geological model of a palaeo-sea, especially if tides were a predominant process at the time of deposition of the sediments. This work highlights the necessity to consider the effects of PBC changes related to relative sea-level variations and their associated impact on tidal dynamics, which will certainly help in improving and refining models of tide-dominated basins and their evolution. This increased knowledge of past basins will help to advance the comprehension of how tidal processes will evolve in response to ongoing sea-level rise.

Acknowledgments

The authors of this paper thank the Norwegian Research Council for their awarded Personal Overseas Research Grant (ref. Number 295061), which allowed the main author to attend Queen's University in Kingston, Canada, as a visiting scholar for 6 months. The Norwegian Research Council is to be further acknowledged for its COTEC grant (ref. Number 295061). Dr. Alexander Rey at Queen's University is recognised for help setting up Delft3D model. JAMG acknowledges funding from the UK Natural Environment Research Council, grant NE/S009566/1 (MATCH). The authors thank Dr Hannah Louise Brooks for her fruitful comments on parts of the manuscripts and its figures, David Hadley-Pryce for his insight on tidal forcing, and Dr Miquel Poyatos-Moré and Dr Anna van Yperen for discussing the impacts that these changes of PBC can have on the sequence stratigraphy of tide-dominated basins

with me. The XXXXXXX reviewers (insert names) who worked on an earlier version of this manuscript are to be sincerely acknowledged for their constructive observations and remarks.

Conflicts of interest

There are no conflicts of interest in the preparation or publication of this work.

Data Availability

All the simulations results and other data presented in this paper (>500Gb) can be saved on an external hard-drive and sent by postal mail.

References

Anderson, T.H. (2015). Jurassic (170–150 Ma) bathe tracks of a continental-scale fault, the Mexico–Alaska megashear, from the Gulf of Mexico to Alaska. In Anderson, T.H., Didenko, A.N., Johnson, C.L., Khanchuk, A.I., & MacDonald, J.H. (Eds.), Late Jurassic margin of Laurasia: a record of faulting accommodating plate rotation, Geological Society of America, Special Paper 513, 107-188.

Anderson, O.J., & Lucas, S.G. (1994). Middle Jurassic stratigraphy, sedimentation and paleogeography in the southern Colorado Plateau and southern High Plains. In: Caputo, M.V., Peterson, J.A., & Franczyk, K.J. (Eds.), Mesozoic Systems of the Rocky Mountain Region, USA, SEPM, Rocky Mountain Section, 299-314.

Anthony, E.J., & Dobroniak, C. (2000). Erosion and recycling of aeolian dunes in a rapidly infilling macrotidal estuary: the Authie, Picardy, northern France. Geological Society, London, Special Publications, 175(1), 109-121.

Anthony, E.J., Mrani-Alaoui, M., & Héquette, A. (2010). Shoreface sand supply and mid-to late Holocene aeolian dune formation on the storm-dominated macrotidal coast of the southern North Sea. Marine Geology, 276(1-4), 100-104.

Arns, A., Wahl, T., Dangendorf, S., & Jensen, J. (2015). The impact of sea level rise on storm surge water levels in the northern part of the German Bight. Coastal Engineering, 96, 118-131.

Ashall, L.M., Mulligan, R.P., Van Proosdij, D., & Poirier, E. (2016). Application and validation of a three-dimensional hydrodynamic model of a macrotidal salt marsh. Coastal Engineering, 114, 35-46.

Bjerrum, C.J., & Dorsey, R.J. (1995). Tectonic controls on deposition of Middle Jurassic strata in a retroarc foreland basin, Utah-Idaho trough, western interior, United States. Tectonics, 14(4), 962-978.

Blackledge, B.W., Green, J.A.M., Barnes, R., & Way, M.J. (2020). Tides on Other Earths: Implications for Exoplanet and Palaeo-Tidal Simulations. Geophysical Research Letters, 47(12), e2019GL085746.

Blakey, R.C. (2014). Paleogeography and paleotectonics of the western interior seaway, Jurassic-Cretaceous of North America. Search and Discovery, 30392, 72.

Blanchard, S., Fielding, C.R., Frank, T.D., & Barrick, J.E. (2016). Sequence stratigraphic framework for mixed aeolian, peritidal and marine environments: Insights from the Pennsylvanian subtropical record of Western Pangaea. Sedimentology, 63(7), 1929-1970.

Brenner, R.L., & Peterson, J.A. (1994). Jurassic sedimentary history of the northern portion of the Western Interior Seaway, USA. In: Caputo, M.V., Peterson, J.A., & Franczyk, K.J. (Eds.), Mesozoic Systems of the Rocky Mountain Region, USA, SEPM, Rocky Mountain Section, 233-272.

Brown, M.M., Mulligan, R.P., & Miller, R.L. (2014). Modeling the transport of freshwater and dissolved organic carbon in the Neuse River Estuary, NC, USA following Hurricane Irene (2011). Estuarine, Coastal and Shelf Science, 139, 148-158.

Burgess, P.M., & Prince, G.D. (2015). Non-unique stratal geometries: implications for sequence stratigraphic interpretations. Basin Research, 27(3), 351-365.

Byrne, H.M., Green, J.A.M., Balbus, S.A., & Ahlberg, P.E. (2020). A key environmental driver of osteichthyan evolution and the fish-tetrapod transition? Proceedings of the Royal Society A, 476(2242), 20200355.

Caputo M.V., & Pryor W.A. (1991). Middle Jurassic tide- and wave-influenced coastal facies and paleogeography, upper San Rafael Group, east-central Utah. In: T.C. Chidsey (Ed.), Geology of East-Central Utah, Utah Geological Association, Salt Lake City, 9-27.

Carless, S.J., Green, J.A.M., Pelling, H.E., & Wilmes, S.B. (2016). Effects of future sea-level rise on tidal processes on the Patagonian Shelf. Journal of Marine Systems, 163, 113-124.

Carr-Crabaugh, M., & Kocurek, G. (1998). Continental sequence stratigraphy of a wet eolian system: a key to relative sea-level change. In: Stanley, K.W., and McCabe, P.J. (Eds.), Relative Role of Eustasy, Climate, and Tectonics in Continental Rocks, SEPM, Special Publication 59, 213-228.

Cartwright, D. (2001). On the origins of knowledge of the sea tides from antiquity to the Thirteenth Century. Earth sciences history, 20(2), 105-126.

Collins, D.S., Avdis, A., Allison, P.A., Johnson, H.D., Hill, J., & Piggott, M.D. (2018). Controls on tidal sedimentation and preservation: Insights from numerical tidal modelling in the Late Oligocene–Miocene South China Sea, Southeast Asia. Sedimentology, 65(7), 2468-2505.

Collins, D.S., Johnson, H.D., & Baldwin, C.T. (2020). Architecture and preservation in the fluvial to marine transition zone of a mixed-process humid-tropical delta: Middle Miocene Lambir Formation, Baram Delta Province, north-west Borneo. Sedimentology, 67(1), 1-46.

Collins, D., Avdis, A., Wells, M.R., Mitchell, A.J., Allison, P.A., Johnson, H.D., Hampson, G.J., Hill, J., Dean, C.D., & Piggott, M. (submitted). Predicting shoreline depositional process regimes using insights from palaeotidal modelling. Earth Science Reviews.

Cosma, M., Finotello, A., Ielpi, A., Ventra, D., Oms, O., D'Alpaos, A., & Ghinassi, M. (2020). Piracy-controlled geometry of tide-dominated point bars: Combined evidence from ancient sedimentary successions and modern channel networks. Geomorphology, 370, 107402.

Costas, S., & FitzGerald, D. (2011). Sedimentary architecture of a spit-end (Salisbury Beach, Massachusetts): The imprints of sea-level rise and inlet dynamics. Marine Geology, 284(1-4), 203-216.

Crabaugh, M., & Kocurek, G. (1993). Entrada Sandstone: an example of a wet aeolian system. In: Pye, K. (Ed.), The Dynamics and Environmental Context of Aeolian Sedimentary Systems, Geological Society of London, Special Publication, 72, 103-126.

Dalrymple, R.W., Duncan, A.M., Ichaso, A.A., & Choi, K.S. (2012). Processes, Morphodynamics, and Facies of Tide-Dominated Estuaries. In: In: Davis, R.A.,Jr., & Dalrymple, R.W. (Eds.), Principles of tidal sedimentology, Dordrecht, Netherlands, Springer Science and Business Media, 187-229.

Danise, S., & Holland, S.M. (2017). Faunal response to sea-level and climate change in a short-lived seaway: Jurassic of the Western Interior, USA. Palaeontology, 60(2), 213-232.

Danise, S., & Holland, S.M. (2018). A sequence stratigraphic framework for the Middle to Late Jurassic of the Sundance Seaway, Wyoming: implications for correlation, basin evolution, and climate change. The Journal of Geology, 126(4), 371-405.

Danise, S., Price, G.D., Alberti, M., & Holland, S.M. (2020). Isotopic evidence for partial geochemical decoupling between a Jurassic epicontinental sea and the open ocean. Gondwana Research, 82, 97-107.

Davies, H. S., Green, J.A., & Duarte, J.C. (2020). Back to the future II: tidal evolution of four supercontinent scenarios. Earth System Dynamics, 11(1), 291-299.

Davis, R.A.,Jr., & Dalrymple, R.W. (Eds.). (2012). Principles of tidal sedimentology, Dordrecht, Netherlands, Springer Science and Business Media, 661 pp.

Dean, C.D., Collins, D.S., van Cappelle, M., Avdis, A., & Hampson, G.J. (2019). Regional-scale paleobathymetry controlled location, but not magnitude, of tidal dynamics in the Late Cretaceous Western Interior Seaway, USA. Geology, 47(11), 1083-1087.

Demko, T.M., Currie, B.S., & Nicoll, K.A. (2004). Regional paleoclimatic and stratigraphic implications of paleosols and fluvial/overbank architecture in the Morrison Formation (Upper Jurassic), Western Interior, USA. Sedimentary Geology, 167(3-4), 115-135.

De Raaf, J.F. M., & Boersma, J.R. (2007). Tidal deposits and their sedimentary structures (seven examples from Western Europe). Netherlands Journal of Geosciences/Geologie en Mijnbouw, 50(3), 479-504.

Doelling, H.H., Sprinkel, D.A., Kowallis, B.J., & Kuehne, P.A. (2013). Temple Cap and Carmel Formations in the Henry Mountains Basin, Wayne and Garfield Counties, Utah. The San Rafael Swell and Henry Mountains Basin—geologic centerpiece of Utah: Utah Geological Association Publication, 42, 279-318.

Elias, E.P.L., Gelfenbaum, G., and Van der Westhuysen, A.J. (2012), Validation of a coupled wave-flow model in a high-energy setting: The mouth of the Columbia River, J. Geophys. Res., 117, C09011.

Eriksson, K.A. (1977). Tidal deposits from the Archaean Moodies Group, Barberton Mountain Land, South Africa. Sedimentary Geology, 18(1-3), 257-281.

Fan, D. (2012). Open-coast tidal flats. In: Davis, R.A.,Jr., & Dalrymple, R.W. (Eds.), Principles of tidal sedimentology, Dordrecht, Netherlands, Springer Science and Business Media, 187-229.

Fang, G., Kwok, Y.K., Yu, K., & Zhu, Y. (1999). Numerical simulation of principal tidal constituents in the South China Sea, Gulf of Tonkin and Gulf of Thailand. Continental Shelf Research, 19(7), 845-869.

Finotello, A., D'Alpaos, A., Bogoni, M., Ghinassi, M., & Lanzoni, S. (2020). Remotely-sensed planform morphologies reveal fluvial and tidal nature of meandering channels. Scientific reports, 10(1), 1-13.

Fritzen, M.R., Cagliari, J., Candido, M., & Lavina, E.L.C. (2019). Tidal bar cyclicity record in the Lower Permian: The Rio Bonito Formation, Paraná Basin, southern Brazil. Sedimentary Geology, 381, 76-83.

Gilluly, J., & Reeside, J.B. Jr. (1928). Sedimentary rocks of the San Rafael Swell and some adjacent areas in eastern Utah. U.S. Geological Survey, Professional Paper 150-D, 61-110.

Green, J.A.M., Huber, M., Waltham, D., Buzan, J., & Wells, M. (2017). Explicitly modelled deep-time tidal dissipation and its implication for Lunar history. Earth and Planetary Science Letters, 461, 46-53.

Green, J.A.M., Molloy, J.L., Davies, H.S., & Duarte, J.C. (2018). Is there a tectonically driven Supertidal cycle?. Geophysical Research Letters, 45(8), 3568-3576.

Green, J.A.M., Davies, H.S., Duarte, J.C., Creveling, J.C., and Scotese, C. (2020). Weak tides during Cryogenian glaciations. Nature Communications, 11, 6227.

Greenberg, D.A., Blanchard, W., Smith, B., & Barrow, E. (2012). Climate change, mean sea level and high tides in the Bay of Fundy. Atmosphere-ocean, 50(3), 261-276.

Gugliotta, M., & Saito, Y. (2019). Matching trends in channel width, sinuosity, and depth along the fluvial to marine transition zone of tide-dominated river deltas: The need for a revision of depositional and hydraulic models. Earth-Science Reviews, 191, 93-113.

Gugliotta, M., Flint, S.S., Hodgson, D.M., & Veiga, G.D. (2015). Stratigraphic record of river-dominated crevasse subdeltas with tidal influence (Lajas Formation, Argentina). Journal of Sedimentary Research, 85(3), 265-284.

Gugliotta, M., Saito, Y., Nguyen, V.L., Ta, T.K.O., Nakashima, R., Tamura, T., ... & Yamamoto, S. (2017). Process regime, salinity, morphological, and sedimentary trends along the fluvial to marine transition zone of the mixed-energy Mekong River delta, Vietnam. Continental Shelf Research, 147, 7-26.

Helland-Hansen, W., & Martinsen, O.J. (1996). Shoreline trajectories and sequences; description of variable depositional-dip scenarios. Journal of Sedimentary Research, 66(4), 670-688.

Helland-Hansen, W., & Hampson, G.J. (2009). Trajectory analysis: concepts and applications. Basin Research, 21(5), 454-483.

Hess, K. (2003). Water level simulation in bays by spatial interpolation of tidal constituents, residual water levels, and datums. Continental Shelf Research, 23(5), 395-414.

Hill, D.F., Griffiths, S.D., Peltier, W.R., Horton, B.P., & Törnqvist, T.E. (2011). High-resolution numerical modeling of tides in the western Atlantic, Gulf of Mexico, and Caribbean Sea during the Holocene. Journal of Geophysical Research, 116, C10014.

Holland, S.M., & Wright, S.N. (2020). The Unconformity That Isn't: A Sequence-Stratigraphic Reinterpretation of the J-5 Unconformity and the Redwater–Windy Hill–Morrison Transition in Wyoming, USA. The Journal of Geology, 128(3), 247-274.

Hori, K., Saito, Y., Zhao, Q., & Wang, P. (2002). Architecture and evolution of the tide-dominated Changjiang (Yangtze) River delta, China. Sedimentary Geology, 146(3-4), 249-264.

Hu, K., Ding, P., Wang, Z., & Yang, S. (2009). A 2D/3D hydrodynamic and sediment transport model for the Yangtze Estuary, China. Journal of Marine Systems, 77(1-2), 114-136.

Idier, D., Paris, F., Le Cozannet, G., Boulahya, F., & Dumas, F. (2017). Sea-level rise impacts on the tides of the European Shelf. Continental Shelf Research, 137, 56-71.

Imlay, R.W. (1947). Marine Jurassic of Black Hills area, South Dakota and Wyoming. American Association of Petroleum Geologists, Bulletin, 31(2), 227-273.

Imlay, R.W. (1952). Correlation of the Jurassic formations of North America, exclusive of Canada. Geological Society of America Bulletin, 63(9), 953-992.

Imlay, R.W. (1980). Jurassic Paleobiogeography of the Conterminous United States in its Continental Setting. U.S. Geological Survey, Professional Paper, 1062, 134 pp.

James, N.P., & Dalrymple, R.W. (Eds.). (2010). Facies Models 4. Geological Association of Canada, 575 pp.

Jensen, P.H., Sprinkel, D.A., Kowallis, B.J., & Brown, K.D. (2016). Geologic Map of the Donkey Flat Quadrangle, Uintah County, Utah. Utah Geological Survey.

Jordan, O.D., & Mountney, N.P. (2010). Styles of interaction between aeolian, fluvial and shallow marine environments in the Pennsylvanian to Permian lower Cutler beds, south-east Utah, USA. Sedimentology, 57(5), 1357-1385.

Jordan, O.D., & Mountney, N.P. (2012). Sequence stratigraphic evolution and cyclicity of an ancient coastal desert system: the Pennsylvanian–Permian Lower Cutler Beds, Paradox Basin, Utah, USA. Journal of Sedimentary Research, 82(10), 755-780.

Kowallis, B.J., Hunt, J.E., Sprinkel, D.A., May, S.B., Bradfield, T.D., & Brown, K.D. (2018). Geologic Map of the Lake Mountain Quadrangle, Uintah County, Utah. Utah Geological Survey, 801, 537-3300.

Kreisa, R.D., & Moila, R.J. (1986). Sigmoidal tidal bundles and other tide-generated sedimentary structures of the Curtis Formation, Utah. Geological Society of America Bulletin, 97(4), 381-387.

Kresning, B., Hashemi, M.R., Neill, S.P., Green, J.M., & Xue, H. (2019). The impacts of tidal energy development and sea-level rise in the Gulf of Maine. Energy, 187, 115942.

Kvale, E.P. (2006). The origin of neap–spring tidal cycles. Marine geology, 235(1-4), 5-18.

Kvale, E.P., & Archer, A.W. (1991). Characteristics of two, Pennsylvanian age, semidiurnal tidal deposits in the Illinois Basin, USA. In: Smith, D.G., Reinson, G.E., Zaitlin, B.A., & Rahmani, R.A. (Eds.), Clastic Tidal Sedimentology, Canadian Society Petroleum Geologists Memories, 16, 79-188.

Longhitano, S.G., Mellere, D., Steel, R.J., & Ainsworth, R.B. (2012). Tidal depositional systems in the rock record: a review and new insights. Sedimentary Geology, 279, 2-22.

Mallinson, D., Culver, S., Leorri, E., Mitra, S., Mulligan, R., & Riggs, S. (2018). Pamlico Sound and the Outer Banks Barrier Islands, North Carolina, USA. In: Moore, L. & Murray, A. (Eds.), Barrier Dynamics and Response to Changing Climate. Cham: Springer, 91-120.

Mansfield, G.R., & Roundy, P.V. (1916). Revision of the Beckwith and Bear River Formations of southeastern Idaho. U.S. Geological Survey, Professional Paper, 98, 75-84

Meyers, S.R., & Malinverno, A. (2018). Proterozoic Milankovitch cycles and the history of the solar system. Proceedings of the National Academy of Sciences, 115(25), 6363-6368.

Mitchell, A.J., Allison, P.A., Gorman, G.J., Piggott, M.D., & Pain, C.C. (2011). Tidal circulation in an ancient epicontinental sea: the Early Jurassic Laurasian Seaway. Geology, 39(3), 207-210.

Mountney, N.P. (2006). Periodic accumulation and destruction of aeolian erg sequences in the Permian Cedar Mesa Sandstone, White Canyon, southern Utah, USA. Sedimentology, 53(4), 789-823.

Müller, R. D., Cannon, J., Qin, X., Watson, R. J., Gurnis, M., Williams, S., Pfaffelmoser, T., Seton, N., Russel, S.H.J., & Zahirovic, S. (2018). GPlates: building a virtual Earth through deep time. Geochemistry, Geophysics, Geosystems, 19(7), 2243-2261.

Mulligan, R.P., Perrie, W., & Solomon, S. (2010). Dynamics of the Mackenzie River plume on the inner Beaufort shelf during an open water period in summer. Estuarine, Coastal and Shelf Science, 89(3), 214-220.

Mulligan, R.P., Walsh, J.P., & Wadman, H.M. (2015). Storm surge and surface waves in a shallow lagoonal estuary during the crossing of a hurricane. Journal of Waterway, Port, Coastal, and Ocean Engineering, 141(4), A5014001.

Mulligan, R.P., Smith, P.C., Tao, J., & Hill, P.S. (2019a). Wind-wave and Tidally Driven Sediment Resuspension in a Macrotidal Basin. Estuaries and Coasts, 42(3), 641-654.

Mulligan, R.P., Mallinson, D.J., Clunies, G.J., Rey, A., Culver, S.J., Zaremba, N., et al. (2019b). Estuarine responses to long-term changes in inlets, morphology and sea level rise. Journal of Geophysical Research: Oceans, 124, 9235-9257.

Mulligan, R.P., Mallinson, D.J., Clunies, G.J., Rey, A., Culver, S.J., Zaremba, N., Leorri, E., & Mitra, S. (2019). Estuarine Responses to Long-Term Changes in Inlets, Morphology, and Sea Level Rise. Journal of Geophysical Research: Oceans, 124(12), 9235-9257.

Parker, B.B. (2007). Tidal analysis and prediction, NOAA Spec. Publ. NOSCO-OPS 3, Silver Spring, Md.

Patterson-Wittstrom, J. (1980). Stratigraphy of the Jurassic Stump Formation. Stratigraphy of Wyoming: 31st Annual Field Conference Guidebook, 91-100.

Pelling, H.E., & Green, J.A.M. (2013). Sea level rise and tidal power plants in the Gulf of Maine. Journal of Geophysical Research: Oceans, 118(6), 2863-2873.

Pelling, H.E., Green, J.A.M., & Ward, S.L. (2013). Modelling tides and sea-level rise: To flood or not to flood. Ocean Modelling, 63, 21-29.

Peterson, F. (1994). Sand dunes, sabkhas, streams, and shallow seas: Jurassic paleography in the southern part of the Western Interior Basin. In: Caputo, M.V., Peterson, J.A., & Franczyk, K.J. (Eds.), Mesozoic Systems of the Rocky Mountain Region, USA, SEPM, Rocky Mountain Section, 233-272.

Phillips, S.P., Howell, J.A., Hartley, A.J., & Chmielewska, M. (2020). Tidal estuarine deposits of the transgressive Naturita Formation (Dakota Sandstone): San Rafael Swell, Utah, USA. Journal of Sedimentary Research, 90(8), 777-795.

Pipiringos, G.N., & O'Sullivan, R.B. (1978). Principal unconformities in Triassic and Jurassic rocks, western interior United States: a preliminary survey. U.S. Geological Survey, Professional Paper, 1035-A, 1-29.

Pipiringos, G.N., & Imlay, R.W. (1979). Lithology and subdivisions of the Jurassic Stump Formation in southeastern Idaho and adjoining areas. Geological Survey, Professional Paper, 1035-C, 1-25.

Räsänen, M.E., Linna, A.M., Santos, J.C., & Negri, F.R. (1995). Late Miocene tidal deposits in the Amazonian foreland basin. Science, 269(5222), 386-390.

van Rijn, L.C. (1993). Principles of sediment transport in rivers, estuaries and coastal seas, Aqua publications, Amsterdam, 790 pp.

Rivers, J. M., Dalrymple, R. W., Yousif, R., Al-Shaikh, I., Butler, J. D., Warren, C., ... & Bari, E. M. A. (2020). Mixed siliciclastic-carbonate-evaporite sedimentation in an arid eolian landscape: The Khor Al Adaid tide-dominated coastal embayment, Qatar. Sedimentary Geology, 408, 105730.

Rossi, V.M., Kim, W., Leva López, J., Edmonds, D., Geleynse, N., Olariu, C., ... & Passalacqua, P. (2016). Impact of tidal currents on delta-channel deepening, stratigraphic architecture, and sediment bypass beyond the shoreline. Geology, 44(11), 927-930.

Simon, B., & Page, J. (2017). Tidal Constituants. Tides, Water Level and Currents Committee, International Hydrographic Organization (https://iho.int/mtg_docs/com_wg/IHOTC/IHOTC_Misc/TWCWG_Constituent_list.pdf).

Sleveland, A.R.N., Midtkandal, I., Galland, O., & Leanza, H.A. (2020). Sedimentary architecture of storm-influenced tidal flat deposits of the upper Mulichinco Formation, Neuquén Basin, Argentina. Frontiers in Earth Science, 8, 219.

Sprinkel, D.A., Doelling, H.H., Kowallis, B.J., Waanders, G., & Kuehne, P.A. (2011). Early results of a study of Middle Jurassic strata in the Sevier fold and thrust belt, Utah. In Sprinkel, D.A., Yonkee, W.A., & Chidsey, T.C. Jr. (Eds.), Sevier Thrust Belt: Northern and Central Utah and Adjacent Areas, Utah Geological Association, Publication 40, 151-172.

Taylor, G.I. (1920). I. Tidal friction in the Irish Sea. Philosophical Transactions of the Royal Society of London. Series A, Containing Papers of a Mathematical or Physical Character, 220(571-581), 1-33.

Thorman, C. H. (2011). The Elko orogeny–A major tectonic event in eastern Nevada–western Utah. Sevier thrust belt—northern and central Utah and adjacent areas. In Sprinkel, D.A., Yonkee, W.A., & Chidsey, T.C. Jr. (Eds.), Sevier Thrust Belt: Northern and Central Utah and Adjacent Areas, Utah Geological Association, Publication 40, 117-129.

Uhlir, D.M., Akers, A., & Vondra, C.F. (1988). Tidal inlet sequence, Sundance formation (upper Jurassic), north-central Wyoming. Sedimentology, 35(5), 739-752.

Waltham, D. (2015). Milankovitch period uncertainties and their impact on cyclostratigraphy. Journal of Sedimentary Research, 85(8), 990-998.

Ward, S.L., Green, J.A.M., & Pelling, H.E. (2012). Tides, sea-level rise and tidal power extraction on the European shelf. Ocean Dynamics, 62(8), 1153-1167.

Ward, S.L., Neill, S.P., Van Landeghem, K.J., & Scourse, J.D. (2015). Classifying seabed sediment type using simulated tidal-induced bed shear stress. Marine Geology, 367, 94-104.

Ward, S.L., Scourse, J.D., Yokoyama, Y., & Neill, S.P. (2020). The challenges of constraining shelf sea tidal models using seabed sediment grain size as a proxy for tidal currents. Continental Shelf Research, 205, 104165.

Wells, M.R., Allison, P.A., Piggott, M.D., Hampson, G.J., Pain, C.C., & Gorman, G.J. (2010). Tidal modeling of an ancient tide-dominated seaway, part 2: the Aptian Lower Greensand seaway of Northwest Europe. Journal of Sedimentary Research, 80(5), 411-439.

Wilcox, W.T., & Currie, B. (2008). Sequence Stratigraphy of the Jurassic Curtis, Summerville, and Stump formations, Eastern Utah and Northwest Colorado. In: Longman, M.W., & Morgan, C.D. (Eds.), Hydrocarbon Systems and Production in the Uinta Basin, Utah, Rocky Mountain Association of Geologists and Utah Geological Association, Publication 37, 9-41.

Yalin, M.S., & Karahan, E. (1979). Inception of sediment transport. Journal of the hydraulics division, 105(11), 1433-1443.

Van Yperen, A.E., Holbrook, J.M., Poyatos-Moré, M., & Midtkandal, I. (2019). Coalesced delta-front sheet-like sandstone bodies from highly avulsive distributary channels: the low-accommodation Mesa Rica Sandstone (Dakota Group, New Mexico, USA). Journal of Sedimentary Research, 89(7), 654-678.

Zuchuat, V., Sleveland, A., Sprinkel, D., Rimkus, A., Braathen, A., & Midtkandal, I. (2018). New insights on the impact of tidal currents on a low-gradient, semi-enclosed, epicontinental basin—the Curtis Formation, east-central Utah, USA. Geology of the Intermountain West, 5, 131-165.

Zuchuat, V., Midtkandal, I., Poyatos-Moré, M., Da Costa, S., Brooks, H.L., Halvorsen, K., ... & Braathen, A. (2019a). Composite and diachronous stratigraphic surfaces in low-gradient, transitional settings: The J-3 “unconformity” and the Curtis Formation, east-central Utah, USA. Journal of Sedimentary Research, 89(11), 1075-1095.

Zuchuat, V., Sleveland, A.R., Pettigrew, R.P., Dodd, T.J., Clarke, S.M., Rabbel, O., ... & Midtkandal, I. (2019b). Overprinted allocyclic processes by tidal resonance in an epicontinental basin: The Upper Jurassic Curtis Formation, east-central Utah, USA. The Depositional Record, 5(2), 272-305.